A BOUNDARY ELEMENT METHOD FOR THE SOLUTION OF LAPLACE'S EQUATION IN THREE-DIMENSIONAL SPACE

by

Y. BULENT YILDIR

A thesis
presented to the University of Manitoba
in partial fulfillment of the
requirements for the degree of
DOCTOR OF PHILOSOPHY
in
ELECTRICAL ENGINEERING

Winnipeg, Manitoba

A BOUNDARY ELEMENT METHOD FOR THE SOLUTION OF LAPLACE'S EQUATION IN THREE-DIMENSIONAL SPACE

BY

Y. BULENT YILDIR

A thesis submitted to the Faculty of Graduate Studies of the University of Manitoba in partial fulfillment of the requirements of the degree of

DOCTOR OF PHILOSOPHY

ABSTRACT

A boundary element method has been developed for the solution of Laplace's equation under Dirichlet, Neumann or mixed boundary conditions in three-dimensional space with piecewise homogeneous media.

The data generation is accomplished by approximating and discretizing the problem geometry utilizing the Coons patch concept with cubic B-spline curves. The technique provides for derivative-continuous geometrical models of free-form surfaces. Various types of blending functions and uni-variate and bi-variate cubic B-spline elements are derived.

The field analysis is effected by exploiting Green's theorem to obtain an integral equation for the potential and its normal derivative on the boundary. The integral equation for each homogeneous region is discretized by using bi-cubic B-spline elements for both the definition of the geometry and the representation of the unknowns. The linear system of equations is obtained through the Bubnov-Galerkin method. The treatment of integrals with Green's function singularity and the numerical integration of nearly singular integrands are described.

Examples of data generation and field solution for a range of problems are given.

ACKNOWLEDGEMENTS

I am grateful and indebted to many people who helped me make this work possible. The large number who influenced my thinking is perhaps best suggested by the references. While it would be impossible to convey the impact all these people have had on the work, I do wish to thank them one and all.

More directly, I would like to express my heartfelt thanks to Dr. L. Shafai without whose encouragment, support and counsel this work wouldn't have been completed. The comments made and the corrections pointed out by Dr. S. Kubina, Prof. E. Bridges, Dr. H. Card and Dr. A. Shah are gratefully acknowledged.

I appreciated the helpful discussions with Dr. S. Bilgen. Thanks also go to Mr. B. Klimpke. Both were there whenever I needed a helping hand. I also acknowledge Dr. A. Wexler's enthusiasm and encouragment.

My parents and Alexis Marjerison are thanked for their unyielding faith in me which was a constant source of inspiration.

The scholarship and leave from the Middle East Technical University, Turkey which enabled me to start and continue this work are gratefully acknowledged.

CONTENTS

LIST OF FIGURES

LIST OF TABLES

Chapter I

INTRODUCTION

Many problems of science and engineering, when reduced to mathematical models, entail the solution of Laplace's equation, $\nabla^2\phi = 0$, in a region D under prescribed boundary conditions on ∂D. Laplace's equation may characterize a number of physical situations in such widely separated areas as electromagnetism, fluid mechanics, heat transfer and acoustics.

Since the inception of Laplace's equation, continuous research has been devoted to developing better methods for its solution. The analytical methods, even today, are rather restricted to problems with simple geometries and homogeneous materials. The numerical methods, on the other hand, offering general applicability have been the object of intense research. Especially, within the last forty years or so, owing to the perpetual advances achieved in the area of high-speed digital computers, various numerical methods have been developed and successfully used to obtain solutions to many boundary value problems including those where Laplace's equation is the governing field equation.

In all of the best known numerical methods applicable for the solution of Laplace's equation, the common concept is the reduction of Laplace's equation or an equivalent integral formulation into a linear system of equations. These methods can be classified in two categories: the methods where approximations are to be made throughout the region D, and the methods where approximations are to be made only on the boundary ∂D. For instance, following the usual nomenclature, the methods of finite differences and finite elements belong to the first category while the boundary element methods belong to the second.

The method of finite differences is among the first numerical techniques developed that offered a broad range of applicability [1],[2]. In this method, utilizing a truncated Taylor series expansion in each coordinate direction, the Laplacian operator is discretized and applied at each point of a rectilinear grid placed on D. The number of unknowns and the number of equations being equal to the number of grid points where no boundary conditions on the potential are given, the resulting system of equations is solved either iteratively or directly. The disadvantages of the method are, among others, the crude modelling of the problem geometry and the large number of unknowns especially in open field problems.

The method of finite elements uses a variational formulation [3],[4],[5]. In this method, the region D is divided into a finite number of non-separated, non-overlapping, very small sub-areas of some prescribed shape which are termed elements. Element geometries and potentials are expressed by polynomials with the nodal values as coefficients. Relating these approximations to Laplace's equation through minimizing a functional that is proportional to the energy of the system yields the values of the solution at the nodes. This method provides better means, i.e. subsectional polynomial approximations, to model the region boundaries. However, in many practical applications the large amount of input data required, the derivative discontinuities in the geometrical model and the inability to model the infinitely extending regions exactly have been the major shortcomings of the method.

The problem of discontinuous derivatives in the geometrical model can probably be eliminated by using the bi-cubic B-spline elements that are derived in Chapter II and infinite elements or a picture frame method may be implemented for open field problems [7], [48]. However, for the large amount of input data required not much can be done other than resorting to some means of automatic data generation. This, in fact, has been one of the objectives of this research; the development of a suitable method of element generation and data preparation. The concept of automatic mesh generation is not new, but we believe that our method is different from previously devised techniques [13], [14] in that it serves both the two-dimensional finite element and three-dimensional boundary element procedures, is based on a subregional scheme and provides for derivative-continuous modelling of the problem geometry. The method is explained in Chapter II.

The methods of the second category solve a boundary integral equation formulation of the problem for some unknowns on ∂D. These methods have been attracting considerable attention for the last twenty years or so because they not only produce precise results with far less input data as compared to the methods of finite differences and finite elements but also cater to the open field problems without any artificial truncation of the region and have the potential of modelling problem geometries accurately. Since the approximations are done only on the boundary, the dimensionality of the problem is reduced by one. Furthermore, being usually bounded and often completely continuous, integral operators as compared to the differential operators, admit a wider selection of trial functions.

Indirect methods of this category solve first for an equivalent source density distribution on ∂D that would sustain the field. Integral equations are derived, utilizing Green's second identity, for the unknown simple or double layer source densities on ∂D and results are obtained through one of the various ways of solving linear operator equations.

Direct methods, on the other hand, do not resort to an intermediate step of determining equivalent source density distributions; they directly solve for the potential and its normal derivative on ∂D. The boundary element method presented in this work is a direct method in the above sense. The boundary integral equation for the unknown potential and its normal derivative is obtained from Green's theorem by taking the field point on ∂D. The surfaces and unknowns are modelled smoothly with bi-cubic B-spline elements, and the linear system of equations is obtained through the Bubnov-Galerkin method. The application of Green's theorem formulation to multi-media problems, unlike indirect methods, produces a block-sparse coefficient matrix. Thus, the implementation of this combination for the solution of Laplace's equation in three-dimensional piecewise homogeneous media results in a novel boundary element method that provides for point sources in the medium and also for equi-potential or equi-gradient parts on boundaries. Furthermore, in this work some new variations of the cubic B-spline elements are derived, compared and the new bi-cubic B-spline element is implemented and tested. Numerical schemes have been adopted for the efficient integration of nearly singular integrands and the evaluation of principal value integrals.

The application of mesh generation and data preparation for a range of problems as well as examples of boundary element method solutions for some field problems with known analytical solutions are demonstrated in Chapter IV.

Chapter II

SURFACE MODELLING

Surface modelling, in the context of this work, refers to the process of approximating and subsequently discretizing a two-dimensional region or a three-dimensional surface into elements. Accurate modelling of the problem region is crucial for both the finite element and the boundary element methods since the boundary normals as well as the Gaussian quadrature points enter the computations in both methods. Moreover, accidental creases in the boundary representations give rise to source concentrations, consequently to erreneous field computations. In most practical problems continuity is required at most up to the second derivative of the unknowns and the boundaries and we therefore choose to employ cubic splines.

2.1 SPLINE APPROXIMATION AND INTERPOLATION

Splines are piecewise polynomial approximating functions that accomodate both interpolatory and smoothness constraints as compared to Lagrangian and Hermitian approximates which cater to interpolatory constraints only [8, p.21]. Cubic splines are those that we shall be interested in. The question leading to the cubic spline approximation is posed as follows.

Given $f_i=f(x_i)$ for $i=1,2,\ldots,N$; f'_1 and f'_N find the curve $s(x)$ such that $s(x_i)=f_i$ for all $i=1,2,\ldots,N$; $s'(x_1)=f'_1$; $s'(x_N)=f'_N$; furthermore $s(x)$ is second order continuous over $[x_1,x_N]$ and agrees with a polynomial of degree not exceeding three over each $[x_i,x_{i+1}]$ where $i=1,2,\ldots,N-1$.

We proceed by expressing the approximating function,

$$s(x) = \sum_{i=0}^{N+1} V_i \, B_i(x) \tag{2.1}$$

where V_i are some constant coefficients to be determined and $B_i(x)$ are the expansion or basis functions to be chosen. Since N+2 conditions are given, $i=0,1,\ldots,N+1$ in the summation.

We intend to choose the expansion functions $B_i(x)$ such that the smoothness constraint is built into them for if each $B_i(x)$ is second order continuous over $[x_1,x_N]$ so will be their linear combination. The set of all polynomials of degree not exceeding three is a four dimensional vector space. Thus only four basis functions are needed on each $[x_i,x_{i+1}]$. Further, each $B_i(x)$ must strech over four subintervals because, otherwise, there won't be exactly four basis functions in each $[x_i,x_{i+1}]$. Hence each $B_i(x)$ is defined piecewise in terms of four at most cubic polynomials which satisfy second order continuity at the subinterval joints. The linearly independent conditions to determine the four parts; $b_{i,1}(x)$, $b_{i,2}(x)$, $b_{i,3}(x)$ and $b_{i,4}(x)$; are

$$\begin{array}{ccccc}
b_{i,1} = 0 & b_{i,1} = b_{i,2} & b_{i,2} = b_{i,3} & b_{i,3} = b_{i,4} & b_{i,4} = 0 \\
b'_{i,1} = 0 & b'_{i,1} = b'_{i,2} & b'_{i,2} = b'_{i,3} & b'_{i,3} = b'_{i,4} & b'_{i,4} = 0 \\
b''_{i,1} = 0 & b''_{i,1} = b''_{i,2} & b''_{i,2} = b''_{i,3} & b''_{i,3} = b''_{i,4} & b''_{i,4} = 0 \\
\hline
x_{i-2} & x_{i-1} & x_i & x_{i+1} & x_{i+2}
\end{array} \qquad (2.2)$$

In addition to the above fifteen equations, we introduce the constraint

$$B_{i-1}(x_i) + B_i(x_i) + B_{i+1}(x_i) = 1 \quad , \qquad (2.3)$$

which only amounts to scaling the basis functions $B_i(x)$. To this end, the right hand side of (2.3) can be any constant. As can be seen from (2.1), scaling up the $B_i(x)$ will result in scaling down the coefficients V_i.

Upon solving for each part, utilizing (2.2) and (2.3), $B_i(x)$ is given in the form

$$B_i(x) = \begin{cases}
0 & x \le x_{i-2} \\
(1/6h^3_{i-2})(x-x_{i-2})^3 & x_{i-2} \le x \le x_{i-1} \\
(1/6h^3_{i-1})[-3(x-x_{i-1})^3 + 3h_{i-1}(x-x_{i-1})^2 + 3h^2_{i-1}(x-x_{i-1}) + h^3_{i-1}] & x_{i-1} \le x \le x_i \\
(1/6h^3_i)[3(x-x_i)^3 - 6h_i(x-x_i)^2 + 4h^3_i] & x_i \le x \le x_{i+1} \\
(1/6h^3_{i+1})[-(x-x_{i+1})^3 + 3h_{i+1}(x-x_{i+1})^2 - 3h^2_{i+1}(x-x_{i+1}) + h^3_{i+1}] & x_{i+1} \le x \le x_{i+2} \\
0 & x_{i+2} \le x
\end{cases} \qquad (2.4)$$

where $h_i = x_{i+1} - x_i$. Different techniques may be used to obtain the solution to the piecewise cubic spline approximation problem. The approach followed here leads to the special class of splines, namely the cubic B-splines [10]. In general, $[x_1, x_N]$ is not equally subdivided and (2.4) are not all of the same shape. When the approximation interval is uniformly meshed, in which case $h_i = h$ (a constant) in (2.4), the uniform cubic B-spline approximation results. The graph of $B_i(x)$ for uniform mesh is shown in Figure 2.1.

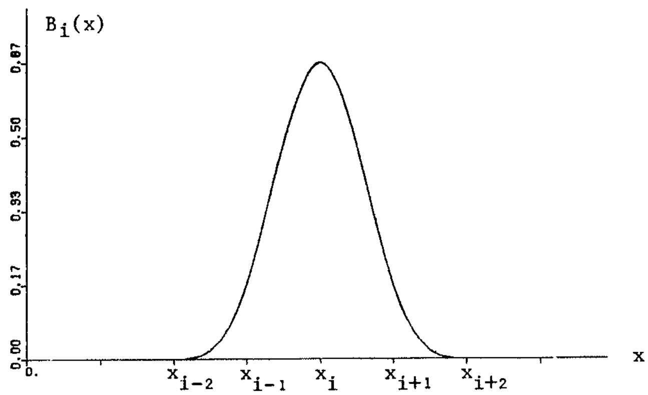

Figure 2.1: B-spline basis function for uniform mesh.

Returning to the approximating function, s(x) must satisfy

$$
\begin{aligned}
f'_1 &= s'(x_1) = \sum_{j=0}^{N+1} V_j \, B'_j(x_1) \\
f'_N &= s'(x_N) = \sum_{j=0}^{N+1} V_j \, B'_j(x_N) \\
f_i &= s(x_i) = \sum_{j=0}^{N+1} V_j \, B_j(x_i) \ , \ i = 1, \ldots\ldots, N \ .
\end{aligned}
\tag{2.5}
$$

The above constraints on s(x) yield a set of N+2 linear equations for the unknowns $V_0, V_1, \ldots, V_{N+1}$. Table 2.1 summarizes the values of $B_i(x)$, $B'_i(x)$ and $B''_i(x)$ at mesh points.

TABLE 2.1

Values of $B_i(x)$ and its derivatives at mesh points

	x_{i-2}	x_{i-1}	x_i	x_{i+1}	x_{i+2}
$B_i(x)$	0	1/6	4/6	1/6	0
$B_i'(x)$	0	1/2h	0	-1/2h	0
$B_i''(x)$	0	$1/h^2$	$-2/h^2$	$1/h^2$	0

The equations resulting from (2.5), in matrix form are

$$\begin{pmatrix} -3/h & 0 & 3/h & 0 \ldots\ldots & & & \\ 1 & 4 & 1 & 0 \ldots\ldots & & & \\ 0 & 1 & 4 & 1 \ldots\ldots & & & \\ \vdots & & & & & & \vdots \\ & & \ldots\ldots 1 & 4 & 1 & 0 & \\ & & \ldots\ldots 0 & 1 & 4 & 1 & \\ & & \ldots\ldots 0 & -3/h & 0 & 3/h & \end{pmatrix} \begin{pmatrix} V_0 \\ V_1 \\ \vdots \\ V_N \\ V_{N+1} \end{pmatrix} = \begin{pmatrix} f_1' \\ f_1 \\ \vdots \\ f_N \\ f_N' \end{pmatrix} \qquad (2.6)$$

Since the coefficient matrix can be partitioned into a linearly independent set of row or column matrices, it is non-singular. Hence the solution of (2.6) yields the unique set of coefficients $V_0, V_1, \ldots, V_{N+1}$ which are also called controlling vertices.

The above construction established the existence of an unique cubic spline, a cubic B-spline, solving the approximation problem. The uniqueness of the cubic splines is proved as follows [8, p.81]. Let there be two cubic spline approximates $s_1(x)$ and $s_2(x)$ satisfying the requirements of the problem. We form $g(x)=s_1(x)-s_2(x)$ which is second order continuous piecewise polynomial and equals zero at N points $x_1, x_2, \ldots, x_N$. Then $g'(x)$ has at least $N-1$ zeros between x_1 and x_N, one per subinterval from Rolle's theorem, plus two more x_1 and x_N by the definition of the problem. It then follows that $g''(x)$ which is a piecewise linear function has at least N zeros, i.e. at least one between each pair of zeros of $g'(x)$. Since there are $N-1$ subintervals in $[x_1, x_N]$ one of them contains two zeros of $g''(x)$ which implies that $g''(x)=0$ there and from the continuity of the second derivative $g''(x)=0$ everywhere. But then $g(x)$ is a linear function in each $[x_i, x_{i+1}]$, $i=1,2,\ldots,N-1$ with zeros at x_i and x_{i+1}, therefore $g(x)=0$ everywhere yielding $s_1(x)=s_2(x)$ and hence proving the uniqueness of cubic spline approximations.

The error associated with cubic spline approximations depends on the smoothness of the function to be approximated. We note the following error bounds from [9].

$$\|f(x) - s(x)\|_2 \le 2\pi^{-2}h^2\|f''(x)\|_2 \tag{2.7}$$

when $f(x) \in C^2[x_1, x_N]$ and

$$\|f(x) - s(x)\|_2 \le 4\pi^{-4}h^4\|f^4(x)\|_2 \tag{2.8}$$

when $f(x) \in C^4[x_1, x_N]$ where $\|\cdot\|_2$ is the L_2 norm and

$$h = \max_{1 \le i \le N-1} (x_{i+1} - x_i) \ . \tag{2.9}$$

The errors are of the same order also in the Tchebycheff norm [8, p.112].

As compared to the piecewise Lagrange and Hermite approximations, splines yield greater smoothness, more favorable error estimates with less number of unknowns. The spline approximates also possess a variation diminishing property [12], that is, they minimize the integral of the square of the second derivative in the case of cubic splines, of the function to be approximated, i.e.

$$\int_{x_1}^{x_N} f''(x)^2\,dx \geq \int_{x_1}^{x_N} s''(x)^2\,dx \ . \tag{2.10}$$

The first derivative information, specified in the problem statement at two extremes, is called end conditions. Second derivative information at the extremes would equally well constitute proper end conditions, in which case the entries of the first and the last rows must be changed with respect to the Table 2.1. The particular choice of zero second derivatives at both ends yields the natural spline fit. These types of splines are called open splines. The closed cubic B-spline is found by solving the N by N system, obtained by deleting the first and the last row in (2.6) and the first and the last columns of the coefficient matrix and setting the entries (1,N) and (N,1) of the resulting matrix to unity.

The above construction of the cubic B-spline approximation is pursued in one dimension. In the case where the approximating function is to be found in multi-dimensional space, s(x) is computed in each coordinate direction.

2.2 THE COONS PATCH

Coons patch is a quadrilateral area of surface defined parametrically through a function which is due to S. A. Coons [11], [17]. The function assumes the boundary curves of the patch to be known and maps the unit square, $U=[0,1]\times[0,1]$, to the surface segment.

Let $P(\xi,\eta)$ denote the Coons patch mapping to be constructed. To this end, select two functions $\beta_0(\cdot)$ and $\beta_1(\cdot)$ such that

$$\beta_0(0) = \beta_1(1) = 1$$
$$\beta_0(1) = \beta_1(0) = 0 \;, \tag{2.11}$$

which have come to be known as blending functions. Consider the surface patch and the unit square in Figure 2.2.

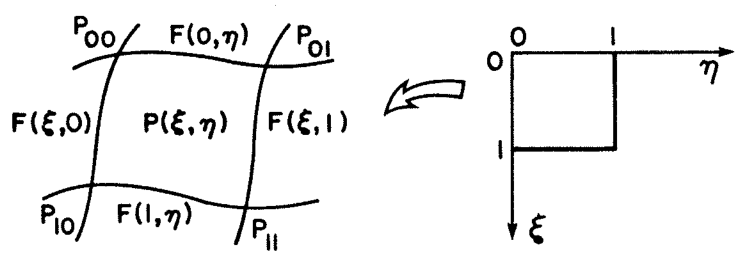

Figure 2.2: Coons patch mapping.

It is evident from Figure 2.2 that the sides $\xi=0$, $\xi=1$, $\eta=0$ and $\eta=1$ are to be mapped onto $F(0,\eta)$, $F(1,\eta)$, $F(\xi,0)$ and $F(\xi,1)$ respectively. To this end, define two mappings

$$T_1(\xi,\eta) = F(0,\eta)\beta_0(\xi) + F(1,\eta)\beta_1(\xi)$$
$$T_2(\xi,\eta) = F(\xi,0)\beta_0(\eta) + F(\xi,1)\beta_1(\eta) \;, \tag{2.12}$$

which are known as lofting operators and the surfaces associated with them are called blended interpolating surfaces or transfinite interpolates since they coincide with the actual surface along entire curves. It is easy to verify that each operator above interpolates to two opposite curves. However, a moment's reflection will indicate that their sum does not interpolate to the boundary of the patch. For instance, $T_1(\xi,\eta)+T_2(\xi,\eta)$ at $\xi=\eta=0$ gives $2P_{00}$ and similarly for the other corners. Nevertheless, we construct a third mapping

$$T_3(\xi,\eta) = P_{00}\beta_0(\xi)\beta_0(\eta) + P_{01}\beta_0(\xi)\beta_1(\eta) + P_{10}\beta_1(\xi)\beta_0(\eta) + P_{11}\beta_1(\xi)\beta_1(\eta) \ , \qquad (2.13)$$

that interpolates to the four corners exactly and subtract $T_3(\xi,\eta)$ from $T_1(\xi,\eta)+T_2(\xi,\eta)$ to obtain

$$\begin{aligned} P(\xi,\eta) = {} & F(0,\eta)\beta_0(\xi) + F(1,\eta)\beta_1(\xi) + F(\xi,0)\beta_0(\eta) + F(\xi,1)\beta_1(\eta) \\ & - P_{00}\beta_0(\xi)\beta_0(\eta) - P_{01}\beta_0(\xi)\beta_1(\eta) \\ & - P_{10}\beta_1(\xi)\beta_0(\eta) - P_{11}\beta_1(\xi)\beta_1(\eta) \ . \end{aligned} \qquad (2.14)$$

It can be shown, by direct substitution, that (2.14) maps the boundary of the unit square onto the boundary of the patch. The mapping (2.14) is also obtainable as the Boolean sum of the operators (2.12), i.e.

$$P(\xi,\eta) = T_1(\xi,\eta) \oplus T_2(\xi,\eta) = T_1(\xi,\eta) + T_2(\xi,\eta) - T_1(\xi,\eta)T_2(\xi,\eta) \ , \qquad (2.15)$$

due to Gordon [15].

For given boundary curves and blending functions, that there is a unique Coons patch is obvious. But what is not obvious is the high order of accuracy of the Coons patch. When $F \in C^4[\Omega]$, where Ω is the global region of definition of F, and the blending functions are cubic splines then

$$\| F(\xi,\eta) - P(\xi,\eta) \| = O(h^8) \quad , \tag{2.16}$$

but if the boundary curves are approximated by cubic splines then the error becomes of $O(h^4)$.

Continuity of the Coons Patch

We wish the mapping (2.14) to match $F(0,\eta)$, $F(1,\eta)$, $F(\xi,0)$ and $F(\xi,1)$ as well as their first and second derivatives and be second order continuous. Since the product and sum of continous functions is continuous, inherent in (2.14) is that, $P(\xi,\eta) \in C^2[U]$ as long as

$$F(0,\eta)\ ,\ F(1,\eta)\ ,\ F(\xi,0)\ ,\ F(\xi,1)\ ,\ \beta_0(\cdot)\ ,\ \beta_1(\cdot) \in C^2[U] \quad , \tag{2.17}$$

where $C^2[U]$ stands for the space of second order continuous functions on the set U. From the Section 2.2, it is known that (2.14) matches the patch boundaries exactly if conditions (2.11) are satisfied. Taking the partial derivatives of (2.14) with respect to ξ and η, it is also easily verified that

$$
\begin{aligned}
&\left.\frac{\partial P(\xi,\eta)}{\partial \xi}\right|_{\eta=0} = F'(\xi,0) &&\left.\frac{\partial^2 P(\xi,\eta)}{\partial \xi^2}\right|_{\eta=0} = F''(\xi,0)\\
&\left.\frac{\partial P(\xi,\eta)}{\partial \xi}\right|_{\eta=1} = F'(\xi,1) &&\left.\frac{\partial^2 P(\xi,\eta)}{\partial \xi^2}\right|_{\eta=1} = F''(\xi,1)\\
&\left.\frac{\partial P(\xi,\eta)}{\partial \eta}\right|_{\xi=0} = F'(0,\eta) &&\left.\frac{\partial^2 P(\xi,\eta)}{\partial \eta^2}\right|_{\xi=0} = F''(0,\eta)\\
&\left.\frac{\partial P(\xi,\eta)}{\partial \eta}\right|_{\xi=1} = F'(1,\eta) &&\left.\frac{\partial^2 P(\xi,\eta)}{\partial \eta^2}\right|_{\xi=1} = F''(1,\eta)
\end{aligned}
\tag{2.18}
$$

$$\frac{\partial^2 P(\xi,\eta)}{\partial \xi\, \partial \eta} = \frac{\partial^2 P(\xi,\eta)}{\partial \eta\, \partial \xi} \quad .$$

To sum up, (2.14) yields a $C^2[U]$ continuous representation of a patch under the conditions (2.11) and (2.17). However not much can be said about the bijectiveness of the mapping because the boundary curves are usually known only at discrete points and the inverse function theorem implies only local invertibility.

We further wish to know the conditions to be met by (2.14) to preserve second order continuity across the interface between adjacent patches. Consider Figure 2.3 where the mappings

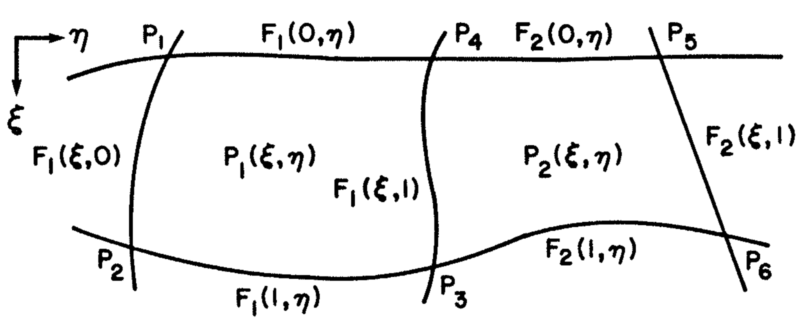

Figure 2.3: Adjacent Coons patches.

$P_1(\xi,\eta)$ and $P_2(\xi,\eta)$ are expressed as

$$P_1(\xi,\eta) = F_1(\xi,0)\beta_0(\eta) + F_1(\xi,1)\beta_1(\eta) + F_1(0,\eta)\beta_0(\xi) + F_1(1,\eta)\beta_1(\xi) - P_1\beta_0(\xi)\beta_0(\eta) - P_2\beta_1(\xi)\beta_0(\eta) - P_3\beta_1(\xi)\beta_1(\eta) - P_4\beta_0(\xi)\beta_1(\eta) \; , \tag{2.19}$$

$$P_2(\xi,\eta) = F_1(\xi,1)\beta_0(\eta) + F_2(\xi,1)\beta_1(\eta) + F_2(0,\eta)\beta_0(\xi) + F_2(1,\eta)\beta_1(\xi) - P_4\beta_0(\xi)\beta_0(\eta) - P_3\beta_1(\xi)\beta_0(\eta) - P_5\beta_1(\xi)\beta_1(\eta) - P_5\beta_0(\xi)\beta_1(\eta) \; . \tag{2.20}$$

We require that

$$\left.\frac{\partial P_1(\xi,\eta)}{\partial \eta}\right|_{\eta=1} = \left.\frac{\partial P_2(\xi,\eta)}{\partial \eta}\right|_{\eta=0} \; . \tag{2.21}$$

Taking the partial derivatives of $P_1(\xi,\eta)$ and $P_2(\xi,\eta)$ and letting

$$\begin{aligned} \beta_0'(1) &= 0 \qquad \beta_0'(0) = 0 \\ \beta_1'(1) &= 0 \qquad \beta_1'(0) = 0 \; , \end{aligned} \tag{2.22}$$

we obtain

$$\left.\frac{\partial P_1(\xi,\eta)}{\partial \eta}\right|_{\eta=1} = F_1'(0,1)\beta_0(\xi) + F_1'(1,1)\beta_1(\xi) \; , \tag{2.23}$$

$$\left.\frac{\partial P_2(\xi,\eta)}{\partial \eta}\right|_{\eta=0} = F_2'(0,0)\beta_0(\xi) + F_2'(1,0)\beta_1(\xi) \; , \tag{2.24}$$

which imply that (2.21) will be satisfied if

$$\begin{aligned} F_1'(0,1) &= F_2'(0,0) \\ F_1'(1,1) &= F_2'(1,0) \; . \end{aligned} \tag{2.25}$$

Similarly differentiating $P_1(\xi,\eta)$ and $P_2(\xi,\eta)$ twice with respect to η at the interface and letting

$$\begin{aligned} \beta_0''(1) &= 0 \qquad \beta_0''(0) = 0 \\ \beta_1''(1) &= 0 \qquad \beta_1''(0) = 0 \; , \end{aligned} \tag{2.26}$$

yields

$$\left.\frac{\partial^2 P_1(\xi,\eta)}{\partial \eta^2}\right|_{\eta=1} = F_1''(0,1)\beta_0(\xi) + F_2''(1,1)\beta_1(\xi) \ , \tag{2.27}$$

$$\left.\frac{\partial^2 P_2(\xi,\eta)}{\partial \eta^2}\right|_{\eta=0} = F_2''(0,0)\beta_0(\xi) + F_2''(1,0)\beta_1(\xi) \ . \tag{2.28}$$

Hence second derivatives at the interface are continuous if

$$\begin{aligned} F_1''(0,1) &= F_2''(0,0) \\ F_1''(1,1) &= F_2''(1,0) \ . \end{aligned} \tag{2.29}$$

Cross-derivatives at the interface, utilizing (2.22), are

$$\left.\frac{\partial^2 P_1(\xi,\eta)}{\partial \xi \ \partial \eta}\right|_{\eta=1} = F_1'(0,1)\beta_0'(\xi) + F_1'(1,1)\beta_1'(\xi) \ , \tag{2.30}$$

$$\left.\frac{\partial^2 P_2(\xi,\eta)}{\partial \xi \ \partial \eta}\right|_{\eta=0} = F_2'(0,0)\beta_0'(\xi) + F_2'(1,0)\beta_1'(\xi) \ , \tag{2.31}$$

and therefore continuous if (2.25) is satisfied.

To sum up, second order continuity will be ensured at the interface if (2.22), (2.25), (2.26) and (2.29) are satisfied. The cross-derivatives will always be zero at the patch corners due to (2.22) thus giving rise to "pseudo-flats" or "thumb-prints". The second partial derivatives will have been forced to be zero at the interface and at the patch corners if the boundary curves are modelled by natural cubic splines.

Blending Functions

We wish to find the blending functions $\beta_0(\cdot)$ and $\beta_1(\cdot)$ subject to

$$\begin{array}{cccc} \beta_0(0) = 1 & \beta_0(1) = 0 & \beta_1(0) = 0 & \beta_1(1) = 1 \\ \beta_0'(0) = 0 & \beta_0'(1) = 0 & \beta_1'(0) = 0 & \beta_1'(1) = 0 \\ \beta_0''(0) = 0 & \beta_0''(1) = 0 & \beta_1''(0) = 0 & \beta_1''(1) = 0 \\ \multicolumn{2}{c}{\beta_0(\cdot)\in C^2[0,1]} & \multicolumn{2}{c}{\beta_1(\cdot)\in C^2[0,1]\ ,} \end{array} \tag{2.32}$$

which are derived in the previous analysis. In the following, first a single polynomial then a cubic spline approximate will be derived that satisfy (2.32).

Polynomial Approximate

There are six conditions to be met by each blending function. We, therefore, choose to approximate them with fifth degree polynomials. Upon imposing (2.32) and then solving for the coefficients, we obtain

$$\begin{aligned} \beta_0(t) &= -\,6t^5 + 15t^4 - 10t^3 + 1 \\ \beta_1(t) &= 6t^5 - 15t^4 + 10t^3 \end{aligned} \tag{2.33}$$

the graphs of which are plotted in Figure 2.4.

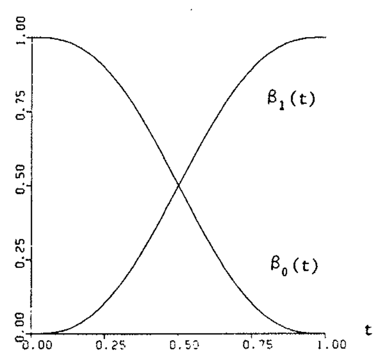

Figure 2.4: Polynomial blending functions.

Cubic Spline Approximate

The least number of segments to satisfy the six constraints is three. Thus, let

$$\beta_0(t) = \begin{cases} \beta_{0,1}(t) & 0 \le t \le 1/3 \\ \beta_{0,2}(t) & 1/3 \le t \le 2/3 \\ \beta_{0,3}(t) & 2/3 \le t \le 1 \,, \end{cases} \tag{2.34}$$

with the conditions

$$\begin{array}{llll} \beta_{0,1} = 1 & \beta_{0,1} = \beta_{0,2} & \beta_{0,2} = \beta_{0,3} & \beta_{0,3} = 0 \\ \beta'_{0,1} = 0 & \beta'_{0,1} = \beta'_{0,2} & \beta'_{0,2} = \beta'_{0,3} & \beta'_{0,3} = 0 \\ \beta''_{0,1} = 0 & \beta''_{0,1} = \beta''_{0,2} & \beta''_{0,2} = \beta''_{0,3} & \beta''_{0,3} = 0 \\ \multicolumn{4}{l}{\beta_{0,1}(t) = a_1t^3 + b_1t^2 + c_1t + d_1 \quad \beta_{0,2}(t) = a_2t^3 + b_2t^2 + c_2t + d_2 \quad \beta_{0,3}(t) = a_3t^3 + b_3t^2 + c_3t + d_3} \\ \hline 0 & 1/3 & 2/3 & 1 \end{array} \tag{2.35}$$

to be met. That $\beta_0(t)+\beta_1(t)=1$ is easily verified. The solution yields

$$\beta_0(t) = \begin{cases} 1/6\ (-27t^3 + 6) & 0 \le t \le 1/3 \\ 1/6\ (54t^3 - 81t^2 + 27t + 3) & 1/3 \le t \le 2/3 \\ 1/6\ (-27t^3 + 81t^2 - 81t + 27) & 2/3 \le t \le 1 \,, \end{cases} \tag{2.36}$$

$$\beta_1(t) = \begin{cases} 1/6\ (27t^3) & 0 \le t \le 1/3 \\ 1/6\ (-54t^3 + 81t^2 - 27t + 3) & 1/3 \le t \le 2/3 \\ 1/6\ (27t^3 - 81t^2 + 81t - 21) & 2/3 \le t \le 1 \,. \end{cases} \tag{2.37}$$

The graphs of the cubic spline blending functions are plotted in Figure 2.5. Coons patch expression with these blending functions is known as the spline blended approximate.

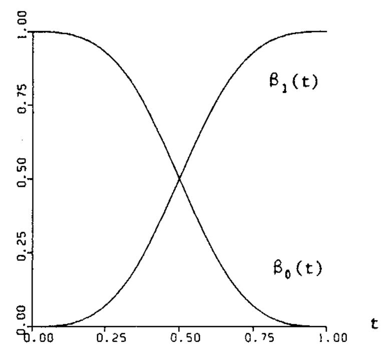

Figure 2.5: Cubic spline blending functions.

Remarks

The disadvantage of the polynomial blending functions, besides being of degree five, is that if integrations of their squares need be calculated then, for exact results, at least six point Gauss-Legendre quadrature would have to be used. Cubic spline blending functions, though they are of lower degree, can not be integrated exactly unless [0,1] is divided into three subintervals. Further, the computation of their values for arbitrary $t \in [0,1]$ first requires the determination of the subinterval where t is situated.

It may be worth noting that in many applications reported in the literature, linear blending functions are used. Let t denote either ξ or η then these functions are simply

$$\begin{aligned} \beta_0(t) &= 1 - t \\ \beta_1(t) &= t \ . \end{aligned} \tag{2.38}$$

Although linear functions are computationally advantageous, not least because of their simplicity, they unfortunately do not satisfy all the conditions in (2.32) and hence may produce derivative discontinuities at patch interfaces even if the boundary curves are second order continuous.

2.3 CUBIC SPLINE ELEMENTS

Here we will be concerned with the derivation of the two-dimensional and the three-dimensional cubic spline elements. In the context of the boundary element method, the two-dimensional element is a section of a curve and a three-dimensional element is a surface patch of quadrilateral shape in this work. Since a curve is a vector-valued function of a single variable, a two-dimensional element is uni-variate. A surface involves two parametric variables, in each coordinate direction and therefore a three-dimensional element is bi-variate.

Two-dimensional Elements

Consider the B-spline basis function (2.4). In $[x_i, x_{i+1}]$, (2.1) reduces to

$$s(x) = B_{i-1}(x)V_{i-1} + B_i(x)V_i + B_{i+1}(x)V_{i+1} + B_{i+2}(x)V_{i+2} , \tag{2.39}$$

and for any x in this subinterval, form the parametric equation

$$x = (x_{i+1} - x_i)\xi + x_i , \tag{2.40}$$

where $0 \le \xi \le 1$. This equation is well-defined for $x_{i+1} - x_i \ne 0$ since

$$\frac{\partial x}{\partial \xi} = (x_{i+1} - x_i) \ne 0 . \tag{2.41}$$

Inserting (2.40) for x into (2.39), we obtain a parametric representation. Denoting $s((x_{i+1}-x_i)\xi+x_i)$ by $P_i(\xi)$ and the portions of the basis functions in (2.4) that lie in $[x_i, x_{i+1}]$ by $\alpha_1(\xi)$, $\alpha_2(\xi)$, $\alpha_3(\xi)$ and $\alpha_4(\xi)$, since these are independent of the subinterval, gives

$$P_i(\xi) = V_{i-1}\alpha_1(\xi) + V_i\alpha_2(\xi) + V_{i+1}\alpha_3(\xi) + V_{i+2}\alpha_4(\xi) \ , \tag{2.42}$$

where

$$\begin{aligned} \alpha_1(\xi) &= (1/6)(-\xi^3+3\xi^2-3\xi+1) \\ \alpha_2(\xi) &= (1/6)(3\xi^3-6\xi^2+4) \\ \alpha_3(\xi) &= (1/6)(-3\xi^3+3\xi^2+3\xi+1) \\ \alpha_4(\xi) &= (1/6)(\xi^3) \ . \end{aligned} \tag{2.43}$$

The expressions in (2.43) are the shape functions for a two-dimensional element. The formula (2.42) interpolates to the spline curve given the subinterval number (element number) and the value of ξ (simplex position). The graphs of the shape functions are given in Figure 2.6.

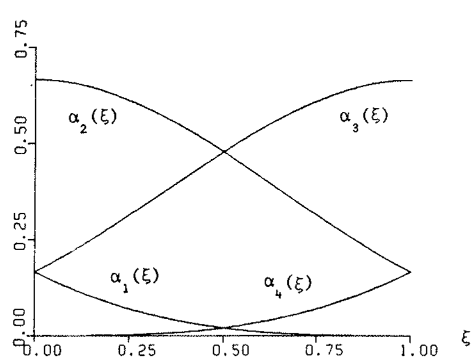

Figure 2.6: Shape functions of the cubic spline element of Type I.

The fact that the uni-variate cubic spline element of Type I is defined through four vertices, which do not necessarily lie on the element, engenders the inconvenience of describing elements by some points in space which, when moved, shape the curve in an uncomfortably predictable manner. To this end, we wish to replace two of the controlling vertices with the two end points of the element. Consider the element in Figure 2.7.

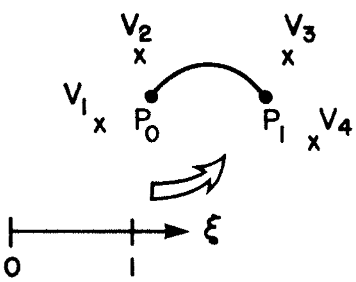

Figure 2.7: Two-dimensional spline element mapping.

From (2.42), we have

$$P(\xi) = V_1\alpha_1(\xi) + V_2\alpha_2(\xi) + V_3\alpha_3(\xi) + V_4\alpha_4(\xi) \quad . \tag{2.44}$$

At ξ=0 and η=1, (2.44) yields

$$\begin{aligned} 6P_0 &= V_1 + 4V_2 + V_3 \\ 6P_1 &= V_2 + 4V_3 + V_4 \quad , \end{aligned} \tag{2.45}$$

which we may use to eliminate any two vertices in terms of P_0 and P_1. Elements of Type II are obtained by eliminating V_2 and V_3. The procedure is to solve for V_2 and V_3 from

(2.45) and substitute in (2.44) to obtain

$$P(\xi) = V_1\{\alpha_1(\xi) - \frac{4}{15}\,\alpha_2(\xi) + \frac{1}{15}\,\alpha_3(\xi)\} + V_4\{\frac{1}{15}\,\alpha_2(\xi) - \frac{4}{15}\,\alpha_3(\xi) + \alpha_4(\xi)\}$$
$$+ P_0\{\frac{24}{15}\,\alpha_2(\xi) - \frac{6}{15}\,\alpha_3(\xi)\} + P_1\{-\frac{6}{15}\,\alpha_2(\xi) + \frac{24}{15}\,\alpha_3(\xi)\}\ . \tag{2.46}$$

The coefficients of V_1, V_4, P_0 and P_1 are the new shape functions. After simplification, their expressions are

$$\begin{aligned}
\gamma_1(\xi) &= -\frac{1}{3}\,\xi^3 + \frac{4}{5}\,\xi^2 - \frac{7}{15}\,\xi \\
\gamma_2(\xi) &= \frac{1}{3}\,\xi^3 - \frac{1}{5}\,\xi^2 - \frac{2}{15}\,\xi \\
\gamma_3(\xi) &= \xi^3 - \frac{9}{5}\,\xi^2 - \frac{1}{5}\,\xi + 1 \\
\gamma_4(\xi) &= -\,\xi^2 + \frac{6}{5}\,\xi^2 + \frac{4}{5}\,\xi\ .
\end{aligned} \tag{2.47}$$

The shape functions (2.47) are plotted in Figure 2.8.

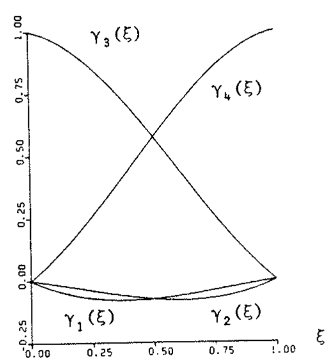

Figure 2.8: Shape functions of the cubic spline element of Type II.

The interpolation formula is then

$$P(\xi) = \sum_{i=1}^{4} T_i\,\gamma_i(\xi)\ , \tag{2.48}$$

where T_1, T_2, T_3 and T_4 are V_1, V_4, P_0 and P_1 respectively.

The vertices V_1 and V_4 could be eliminated instead of V_2 and V_3. Solving for V_1 and V_4 from (2.45) and substituting into (2.44) yields

$$P(\xi) = V_2\{-4\alpha_1(\xi)+\alpha_2(\xi)-\alpha_4(\xi)\} + V_3\{-\alpha_1(\xi)+\alpha_3(\xi)-4\alpha_4(\xi)\} + 6\alpha_1(\xi)P_0 + 6\alpha_4(\xi)P_1 \quad . \tag{2.49}$$

The coefficients of V_2, V_3, P_0 and P_1 are the new shape functions which we shall denote by f_1, f_2, f_3 and f_4, respectively. After simplification

$$\begin{aligned} f_1(\xi) &= \xi^3 - 3\xi^2 + 2\xi \\ f_2(\xi) &= -\xi^3 + \xi \\ f_3(\xi) &= -\xi^3 + 3\xi^2 - 3\xi + 1 \\ f_4(\xi) &= \xi^3 \ . \end{aligned} \tag{2.50}$$

The shape functions (2.50) are plotted in Figure 2.9.

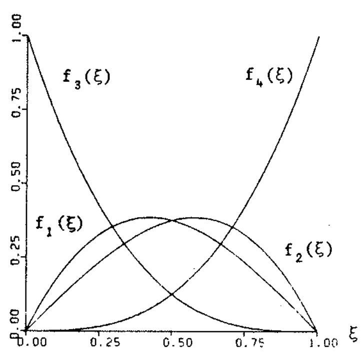

Figure 2.9: Shape functions of the cubic spline element of Type III.

The interpolation formula is then

$$P(\xi) = \sum_{i=1}^{4} G_i \, f_i(\xi) \ , \tag{2.51}$$

where G_1, G_2, G_3 and G_4 are V_2, V_3, P_0 and P_1 respectively.

We may go further and replace all vertices in terms of points on the element. Locating two more points P_2 and P_3 corresponding to $\xi=1/3$ and $\xi=2/3$ respectively we obtain

$$\begin{aligned} 27P_2 - 8P_0 - 10V_2 - P_1 &= 8V_3 \\ 27P_3 - P_0 - 8V_2 - 8P_1 &= 10V_3 , \end{aligned} \tag{2.52}$$

in addition to (2.45). Solving for the vertices from (2.52) and (2.45) yields

$$\begin{aligned} 2V_2 &= 15P_2 - 12P_3 - 4P_0 + 3P_1 \\ 2V_3 &= 15P_3 - 12P_2 - 3P_0 - 4P_1 \\ 2V_1 &= 25P_0 - 48P_2 + 33P_3 - 8P_1 \\ 2V_4 &= 25P_1 + 33P_2 - 48P_3 - 8P_0 , \end{aligned} \tag{2.53}$$

and substituting (2.53) in (2.44) we obtain four new shape functions

$$\begin{aligned} \ell_1(\xi) &= \frac{1}{2}\,(2 - 11\xi + 18\xi^2 - 9\xi^3) \\ \ell_2(\xi) &= \frac{1}{2}\,(9\xi^3 - 9\xi^2 + 2\xi) \\ \ell_3(\xi) &= \frac{9}{2}\,(3\xi^3 - 5\xi^2 + 2\xi) \\ \ell_4(\xi) &= \frac{9}{2}\,(-3\xi^3 + 4\xi^2 - \xi) , \end{aligned} \tag{2.54}$$

with the interpolation formula

$$P(\xi) = \sum_{i=1}^{4} P_i\, \ell_i(\xi) . \tag{2.55}$$

A moment's reflection will reveal that these are in fact the shape functions of the uni-variate cubic Lagrangian element. The graphs of the shape functions are plotted in Figure 2.10.

We thus have shown that for every boundary curve representable by cubic spline elements there is an identical representation with the cubic Lagrangian elements which can be explained by the fact that the cubic splines constitute a proper subset of the piecewise cubic Lagrangian polynomials over the same partitioning of $[x_1, x_N]$.

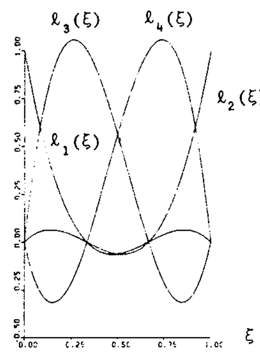

Figure 2.10: Shape functions of the cubic Lagrangian element.

Remarks

The uni-variate elements above are used in the derivation of the bi-variate elements in the next section but they are also usable in two-dimensional boundary element methods. As regards the rational choice of elements, the properties required of them are that the coordinate functions formed by the combination of the shape functions associated with the elements be almost orthonormal or at least strongly minimal and that the representations they provide involve only points on the boundary. The first requirement is due to Mikhlin [35, p.132] where he establishes it as a necessary and sufficient condition for the stability of the Ritz and

Bubnov-Galerkin methods and the second requirement is to provide direct access to the boundary description. With respect to the second requirement, cubic Lagrangian element representation is more desirable than the others for it contains only points on the boundary. For the first requirement, a fair approach would be to compare the representations on a per element basis since in that case each coordinate system spans the same space. For each set, using the norm and inner product definitions,

$$\|u\|_2 = \left[\int_0^1 u(\xi)^2 \, d\xi \right]^{\frac{1}{2}}$$
$$\langle u,v \rangle_2 = \int_0^1 u(\xi)\cdot v(\xi)\, d\xi = \|u\|_2 \|v\|_2 \cos\theta_{u,v} \quad , \tag{2.56}$$

the magnitudes of the shape functions and the angles between each pair of them are computed and given in Table 2.2 where the angles are in degrees and the entries in the first column refer to shape function numbers. Clearly, the cubic Lagrangian element satisfies the desirable properties the most.

It is possible to orthonormalize the shape functions of each set by Gram-Schmidt procedure, however the element definitions will not include points on the boundary. For instance, for linear Lagrangian elements with end points P_0 and P_1, we have $\alpha_1(\xi)=\xi$, $\alpha_2(\xi)=1-\xi$ and $P(\xi)=P_0\xi-P_1(1-\xi)$. Through Gram-Schmidt process we obtain $\bar{\alpha}_1=\sqrt{3}\xi$ and $\bar{\alpha}_2=2-3\xi$ with $P(\xi)=C_1\bar{\alpha}_1(\xi)+C_2\bar{\alpha}_2(\xi)$ where $C_1=(2P_1+P_0)/2\sqrt{3}$ and $C_2=P_0/2$.

TABLE 2.2

Magnitudes and angles for uni-variate shape functions

Magnitudes	Type I	Type II	Type III	Lagrange
(1)	.0629941	.0559667	.2760262	.2760262
(2)	.4855042	.0559667	.2760262	.2760262
(3)	.4855042	.6357598	.3779645	.6210590
(4)	.0629941	.6357598	.3779645	.6210590
Angles				
(1,2)	33.18	23.72	14.36	81.46
(1,3)	67.09	151.18	56.79	69.89
(1,4)	87.13	134.24	65.75	97.18
(2,3)	38.25	134.24	65.75	97.18
(2,4)	67.09	151.18	56.79	69.89
(3,4)	33.18	60.05	87.13	82.82

Three-dimensional Elements

Bi-variate spline elements are derived from the Coons patch expression. The edges of a surface patch can be thought of as uni-variate boundary curves and as such they can be expressed by any one of the four uni-variate elements developed in the previous section. Insertion of a particular edge representation into the Coons patch expression thus yields a different bi-variate element. If the edges are expressed with uni-variate elements of Type I, one obtains the bi-cubic spline element of Type I with 16 vertices none of which may lie on the surface. Therefore this element is not continued. Representing the patch edges with the uni-variate elements of Type II we obtain the bi-cubic spline element of Type II. The patch model is shown in Figure 2.11.

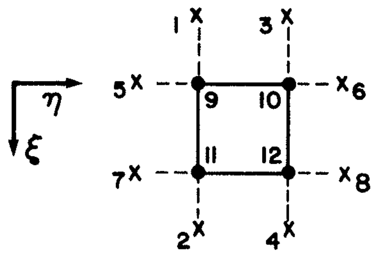

Figure 2.11: Patch model for bi-cubic spline element of Type II.

The patch interpolation formula after simplification becomes

$$P(\xi,\eta) = \sum_{i=1}^{12} V_i A_i(\xi,\eta) \quad , \tag{2.57}$$

with the shape functions

$$\begin{aligned}
A_1(\xi,\eta) &= \alpha_1(\xi)\ \beta_0(\eta) - \tfrac{4}{15}\alpha_2(\xi)\ \beta_0(\eta) + \tfrac{1}{15}\alpha_3(\xi)\ \beta_0(\eta) \\
A_2(\xi,\eta) &= \alpha_4(\xi)\ \beta_0(\eta) + \tfrac{1}{15}\alpha_2(\xi)\ \beta_0(\eta) - \tfrac{4}{15}\alpha_3(\xi)\ \beta_0(\eta) \\
A_3(\xi,\eta) &= \alpha_1(\xi)\ \beta_1(\eta) - \tfrac{4}{15}\alpha_2(\xi)\ \beta_1(\eta) + \tfrac{1}{15}\alpha_3(\xi)\ \beta_1(\eta) \\
A_4(\xi,\eta) &= \alpha_4(\xi)\ \beta_1(\eta) + \tfrac{1}{15}\alpha_2(\xi)\ \beta_1(\eta) - \tfrac{4}{15}\alpha_3(\xi)\ \beta_1(\eta) \\
A_5(\xi,\eta) &= \alpha_1(\eta)\ \beta_0(\xi) - \tfrac{4}{15}\alpha_2(\eta)\ \beta_0(\xi) + \tfrac{1}{15}\alpha_3(\eta)\ \beta_0(\xi) \\
A_6(\xi,\eta) &= \alpha_4(\eta)\ \beta_0(\xi) + \tfrac{1}{15}\alpha_2(\eta)\ \beta_0(\xi) - \tfrac{4}{15}\alpha_3(\eta)\ \beta_0(\xi) \\
A_7(\xi,\eta) &= \alpha_1(\eta)\ \beta_1(\xi) - \tfrac{4}{15}\alpha_2(\eta)\ \beta_1(\xi) + \tfrac{1}{15}\alpha_3(\eta)\ \beta_1(\xi) \\
A_8(\xi,\eta) &= \alpha_4(\eta)\ \beta_1(\xi) + \tfrac{1}{15}\alpha_2(\eta)\ \beta_1(\xi) - \tfrac{4}{15}\alpha_3(\eta)\ \beta_1(\xi) \\
A_9(\xi,\eta) &= -6\beta_0(\xi)\ \beta_0(\eta) + \tfrac{24}{15}\alpha_2(\xi)\ \beta_0(\eta) - \tfrac{6}{15}\alpha_3(\xi)\ \beta_0(\eta) \\
&\quad + \tfrac{24}{15}\alpha_2(\eta)\ \beta_0(\xi) - \tfrac{6}{15}\alpha_3(\eta)\ \beta_0(\xi) \\
A_{10}(\xi,\eta) &= -6\beta_0(\xi)\ \beta_1(\eta) + \tfrac{24}{15}\alpha_2(\xi)\ \beta_1(\eta) - \tfrac{6}{15}\alpha_3(\xi)\ \beta_1(\eta) \\
&\quad + \tfrac{24}{15}\alpha_3(\eta)\ \beta_0(\xi) - \tfrac{6}{15}\alpha_2(\eta)\ \beta_0(\xi) \\
A_{11}(\xi,\eta) &= -6\beta_1(\xi)\ \beta_0(\eta) + \tfrac{24}{15}\alpha_3(\xi)\ \beta_0(\eta) - \tfrac{6}{15}\alpha_2(\xi)\ \beta_0(\eta) \\
&\quad + \tfrac{24}{15}\alpha_2(\eta)\ \beta_1(\xi) - \tfrac{6}{15}\alpha_3(\eta)\ \beta_1(\xi) \\
A_{12}(\xi,\eta) &= -6\beta_1(\xi)\ \beta_1(\eta) + \tfrac{24}{15}\alpha_3(\xi)\ \beta_1(\eta) - \tfrac{6}{15}\alpha_2(\xi)\ \beta_1(\eta) \\
&\quad + \tfrac{24}{15}\alpha_3(\eta)\ \beta_1(\xi) - \tfrac{6}{15}\alpha_2(\eta)\ \beta_1(\xi) \ ,
\end{aligned} \tag{2.58}$$

the graphs of which are shown in Figure 2.12.

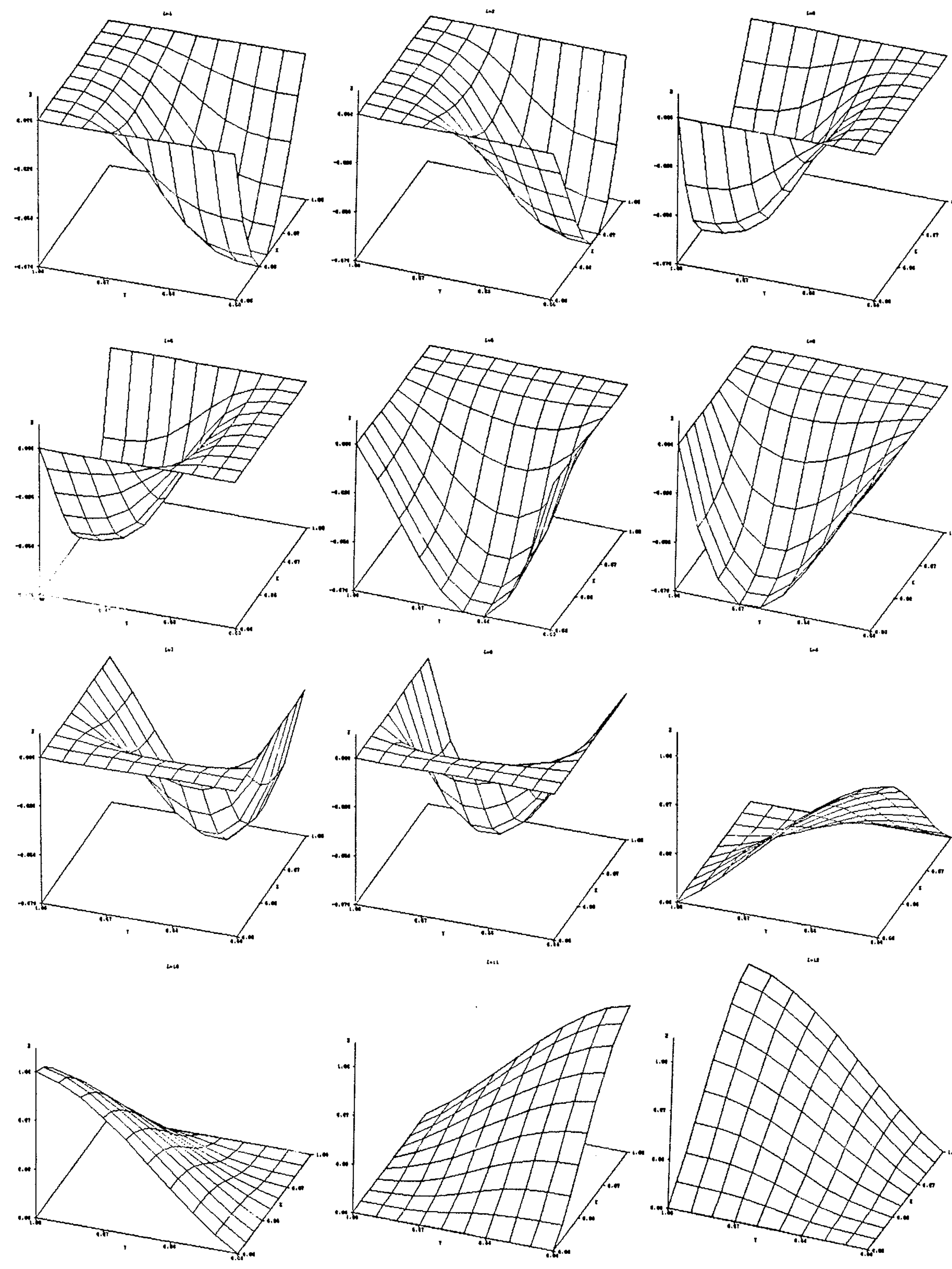

Figure 2.12: Shape functions of bi-cubic spline element of Type II.

Choosing uni-variate elements of Type III to express the patch edges we obtain bi-cubic spline element of Type III the patch model for which is again the one shown in Figure 2.11 except that the extension vertices this time are the ones associated with the corner nodes. The patch interpolation formula is then

$$P(\xi,\eta) = \sum_{i=1}^{12} Q_i \, B_i(\xi,\eta) \quad , \tag{2.59}$$

where the shape functions are

$$\begin{aligned}
B_1(\xi,\eta) &= \beta_0(\eta)[-4\alpha_1(\xi) + \alpha_2(\xi) - \alpha_4(\xi)] \\
B_2(\xi,\eta) &= \beta_0(\eta)[-\alpha_1(\xi) + \alpha_3(\xi) - 4\alpha_4(\xi)] \\
B_3(\xi,\eta) &= \beta_1(\eta)[-4\alpha_1(\xi) + \alpha_2(\xi) - \alpha_4(\xi)] \\
B_4(\xi,\eta) &= \beta_1(\eta)[-\alpha_1(\xi) + \alpha_3(\xi) - 4\alpha_4(\xi)] \\
B_5(\xi,\eta) &= \beta_0(\xi)[-4\alpha_1(\eta) + \alpha_2(\eta) - \alpha_4(\eta)] \\
B_6(\xi,\eta) &= \beta_0(\xi)[-\alpha_1(\eta) + \alpha_3(\eta) - 4\alpha_4(\eta)] \\
B_7(\xi,\eta) &= \beta_1(\xi)[-4\alpha_1(\eta) + \alpha_2(\eta) - \alpha_4(\eta)] \\
B_8(\xi,\eta) &= \beta_1(\xi)[-\alpha_1(\eta) + \alpha_3(\eta) - 4\alpha_4(\eta)] \\
B_9(\xi,\eta) &= \beta_0(\eta)[6\alpha_1(\xi)] + \beta_0(\xi)[6\alpha_1(\eta)] - \beta_0(\xi)\beta_0(\eta) \\
B_{10}(\xi,\eta) &= \beta_1(\eta)[6\alpha_1(\xi)] + \beta_0(\xi)[6\alpha_4(\eta)] - \beta_0(\xi)\beta_1(\eta) \\
B_{11}(\xi,\eta) &= \beta_0(\eta)[6\alpha_4(\xi)] + \beta_1(\xi)[6\alpha_1(\eta)] - \beta_1(\xi)\beta_0(\eta) \\
B_{12}(\xi,\eta) &= \beta_1(\eta)[6\alpha_4(\xi)] + \beta_1(\xi)[6\alpha_4(\eta)] - \beta_1(\xi)\beta_1(\eta) \quad ,
\end{aligned} \tag{2.60}$$

the graphs of which are shown in Figure 2.13.

Expressing the patch edges with uni-variate elements of Type IV, we obtain the bi-variate cubic spline blended ele-

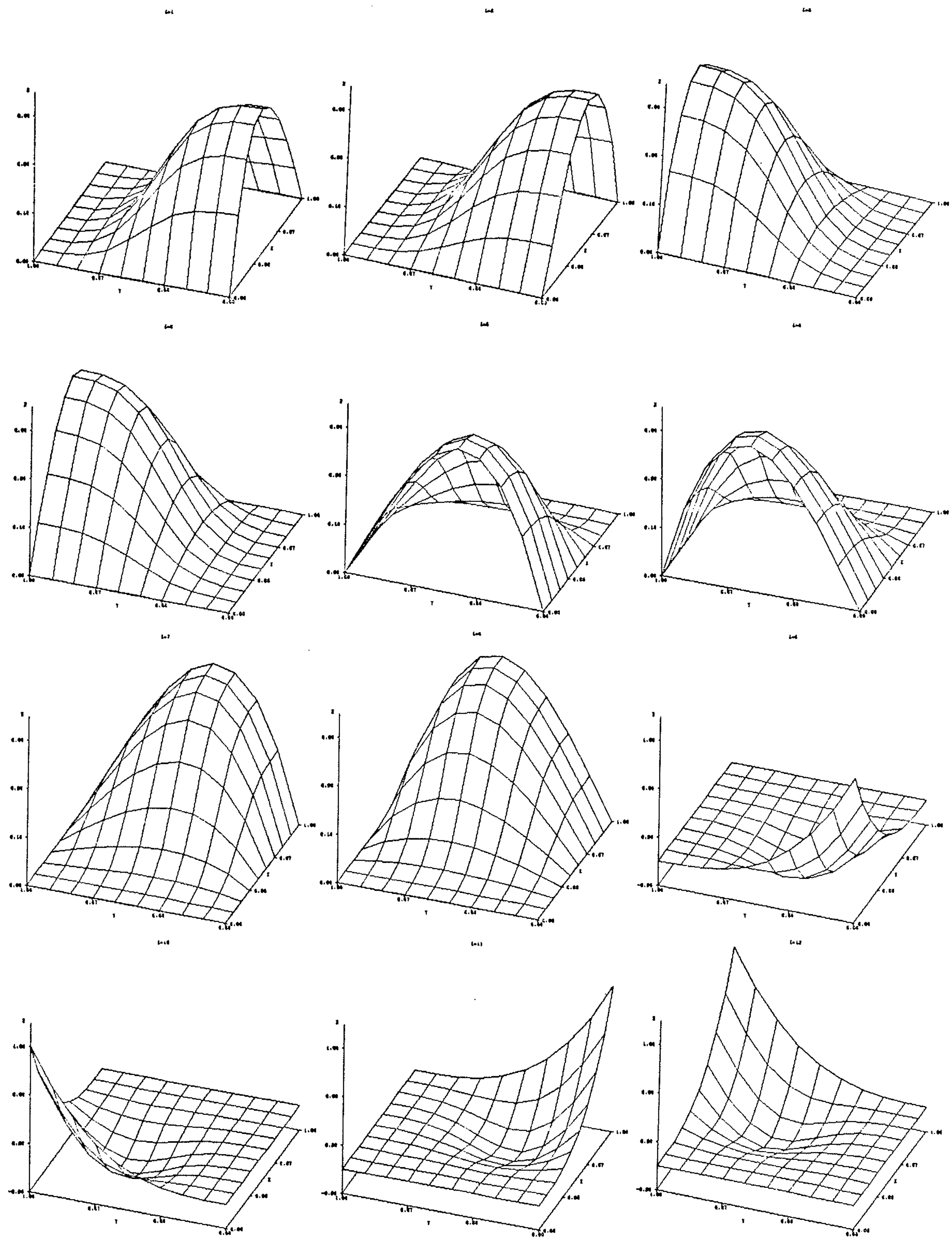

Figure 2.13: Shape functions of bi-cubic spline element of Type III.

ment of Type IV the patch model for which is shown in Figure 2.14. The interpolation formula is given by

$$P(\xi,\eta) = \sum_{i=1}^{12} P_i \, L_i(\xi,\eta) \tag{2.61}$$

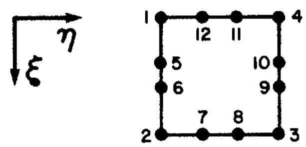

Figure 2.14: Patch model for the bi-variate element of Type IV.

where the shape functions are

$$\begin{aligned}
L_1(\xi,\eta) &= \beta_0(\eta)\ell_1(\xi) + \beta_0(\xi)\ell_1(\eta) - \beta_0(\xi)\,\beta_0(\eta) \\
L_2(\xi,\eta) &= \beta_0(\eta)\ell_2(\xi) + \beta_1(\xi)\ell_1(\eta) - \beta_1(\xi)\,\beta_0(\eta) \\
L_3(\xi,\eta) &= \beta_1(\eta)\ell_2(\xi) + \beta_1(\xi)\ell_2(\eta) - \beta_1(\xi)\,\beta_1(\eta) \\
L_4(\xi,\eta) &= \beta_1(\eta)\ell_1(\xi) + \beta_0(\xi)\ell_2(\eta) - \beta_0(\xi)\,\beta_1(\eta) \\
L_5(\xi,\eta) &= \beta_0(\eta)\ell_3(\xi) \\
L_6(\xi,\eta) &= \beta_0(\eta)\ell_4(\xi) \\
L_7(\xi,\eta) &= \beta_1(\xi)\ell_3(\eta) \\
L_8(\xi,\eta) &= \beta_1(\xi)\ell_4(\eta) \\
L_9(\xi,\eta) &= \beta_1(\eta)\ell_4(\xi) \\
L_{10}(\xi,\eta) &= \beta_1(\eta)\ell_3(\xi) \\
L_{11}(\xi,\eta) &= \beta_0(\xi)\ell_4(\eta) \\
L_{12}(\xi,\eta) &= \beta_0(\xi)\ell_3(\eta) \; ,
\end{aligned} \tag{2.62}$$

with the graphs shown in Figure 2.15.

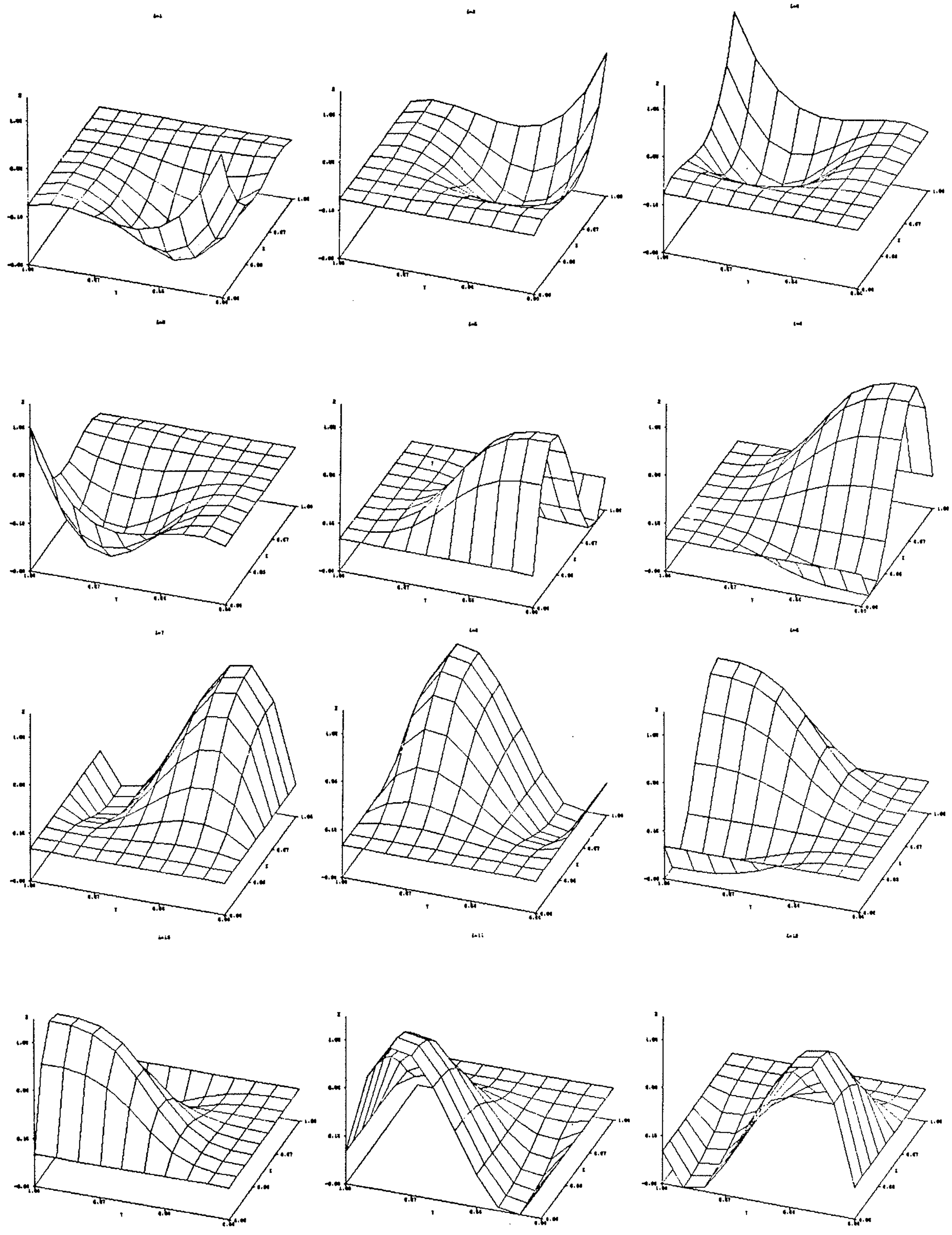

Figure 2.15: Shape functions of bi-cubic blended element.

The properties required of the shape functions for uni-variate elements also apply to bi-variate elements. The magnitudes and angles for bi-cubic spline elements are computed using

$$\|u\|_2 = \left[\int_0^1 \int_0^1 u(\xi,\eta)^2 d\xi \; d\eta \right]^{\frac{1}{2}}$$

$$< u,v >_2 = \int_0^1 \int_0^1 u(\xi,\eta) \; v(\xi,\eta) d\xi \; d\eta = \|u\|_2 \|v\|_2 \cos\theta_{u,v} \quad , \tag{2.63}$$

and shown in Table 2.3. The cubic Serendipity element [4, p.88] results when linear blending functions (2.38) are used with the Type IV element. It then follows, from Section 2.2, that the cubic Serendipity element representation does not ensure derivative continuity at element interfaces even if the boundary curves are second order continuous.

The element of Type IV satisfies the desirable properties the most and Type III is preferred to Type II not only because of the above criteria but also since it models the geometry with the least number of vertices. For instance, a flat rectangular patch is modelled with four corner nodes by Type III element while Type II element requires 12 vertices. However, in problems where the field variation is of higher order than cubic all vertices should be freed for best results, as will be demonstrated in Chapter IV.

TABLE 2.3

Magnitudes and angles for bi-variate shape functions

Magnitudes	Type II	Type III	Type IV	Serendip
(1)-(4)	.0356160	.1756591	.2528860	.2023178
(5)-(8)	.0356160	.1756591	.3952330	.3585685
(9)-(12)	.4042870	.1327614	.3952330	.3585685
Angles				
(1,2)	23.71	14.36	68.61	46.04
(1,3)	76.43	76.43	82.68	59.15
(1,4)	77.59	76.86	68.61	46.04
(1,5)	47.71	52.12	142.61	131.28
(1,6)	61.40	59.92	97.78	109.33
(1,7)	61.40	59.92	104.75	119.01
(1,8)	70.09	65.85	92.00	101.79
(1,9)	149.78	94.55	92.00	101.79
(1,10)	108.65	99.85	104.75	119.01
(1,11)	133.56	97.50	97.78	109.33
(1,12)	104.18	98.92	142.61	131.28

2.4 MESH GENERATION

The Coons patch concept together with the B-spline approximation and interpolation technique suggest an efficient scheme for mesh generation. Consider, first in two dimensions, a region of quadrilateral shape. The unit square $[0,1]\times[0,1]$ can be meshed into a grid of required form and mapped to the region by the Coons patch expression. Figure 2.16 shows, by way of example, two such mappings.

In three dimensions the region is a quadrilateral patch on the surface. Thus, the only difference between the two-dimensional finite element and three-dimensional boundary element generations is that the mapping in the latter case has to be repeated for one more dimension.

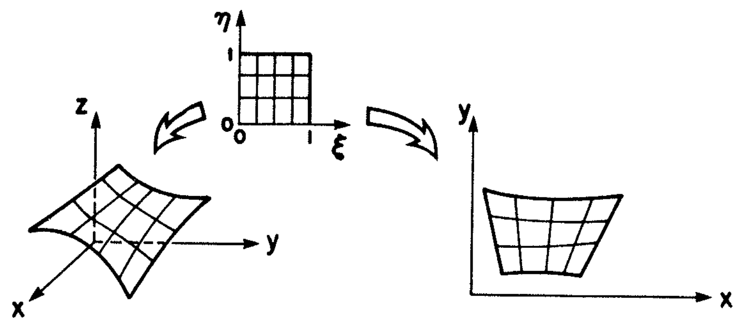

Figure 2.16: Mesh generation through Coons patch mapping.

The region to be discretized is first divided into a number of quadrilateral subregions with or without curved edges as required. This first level subdivision, which is usually done in order to comply with the different material properties and boundary conditions, is assumed to have been performed prior to the automatic data preparation.

In the mesh generation step, which proceeds subregion by subregion, each edge that is defined through a set of spatial coordinates of points on it, is modelled by an open cubic spline curve. The locations of the required number of nodes on an edge are then found by interpolation, using (2.1). Since the edges are modelled parametrically, multiple-valued curves pose no difficulty.

For the interpolations are from the one-dimensional simplex [0,1] to each one of the global coordinates, the number of points to be interpolated per span, i.e. for each interval, as well as the corresponding simplex locations must be determined. To this end, if M is the degree of elements [3], J is the number of points that define the edge and L is the number of initial nodes required then the smallest K for which

$$\frac{M*(L+1)*K}{J-1}*(J-1) = M*(L+1) \ , \tag{2.64}$$

where all symbols are integers, is sought. When such a K is found then the number of points to be interpolated per span, N, is

$$N = \frac{M*(L+1)}{J-1} - 1 \ , \tag{2.65}$$

and the simplex coordinates are $\xi=i/(N+1)$, $i=1,2,...,N$ for each span. On the total there will be N*(L+1)+L+2 number of points available on the edge, the first and every K'th one of which will be an initial or a mid-side node.

Once the nodes on the edges are located, the Coons patch expression (2.14) is used to compute the global coordinates of the nodes interior to the subregion. To this end, the unit square is meshed into a rectangular grid with the local coordinates of the interior mesh points being

$$\left\{(\xi_i,\eta_j)\right\}_{i=2,j=2}^{N+1\ \ I+1} \equiv \left\{\frac{i}{N+1}\right\}_{i=1}^{N} \times \left\{\frac{i}{I+1}\right\}_{j=1}^{I} \ , \tag{2.66}$$

where there are assumed to be N+2 points in the ξ-direction and I+2 points in the η-direction. Triangular elements may be generated by bisecting quadrilateral elements along the shorter diagonal for better aspect ratio. A triangular subregion causes no problem for it can be treated as a special case of a quadrilateral subregion. After all subregions are done, the node and element lists are prepared by reprocessing the elements.

The edges of the subregions are assumed to have been entered in the counter-clockwise sequence. To check this and also to determine if the diagonal of bisection, in the generation of triangles, lies within the quadrilateral a test is performed. In two dimensions the expression

$$c = (x_1 - x_2)(y_3 - y_2) - (x_3 - x_2)(y_1 - y_2) \quad , \qquad (2.67)$$

where (x_1, y_1), (x_2, y_2) and (x_3, y_3) are the triangle vertices, is positive, zero or negative whenever the sequence is clockwise, the vertices coincide or the sequence is counter-clockwise. In three dimensions, if the origin does not lie in the plane of the triangle then

$$c = - N_x M_x - N_y M_y - N_z M_z \quad , \qquad (2.68)$$

where N_x, N_y, N_z are the components of the normal to the triangle, pointing away from the region that contains the origin, and M_x, M_y, M_z are the components of the vector from the origin to the center of the triangle, is negative, zero or positive whenever the sequence is clockwise, the vertices coincide or the sequence is counter-clockwise. The above formulae can also be exploited to perform point-in-region or point-on-surface searches.

The region after being modelled is displayed for inspection. In three dimensions, a perspective transformation [18], is employed prior to the plotting. The geometrical description data is then interfaced to the particular application program. Various interfacing programs have been developed for this purpose [55].

As for continuity, from the results of Section 2.2 it is clear that the subregions are second order continuous as long as the blending functions and the boundary curves are. Across subregion interfaces, first and second derivative continuity depends on the respective derivative continuity betweeen boundary curves. If natural B-splines are used to approximate the boundary curves the second derivatives across subregion interfaces will be zero and the first derivatives may be discontinuous. Second order continuity may be ensured, if an edge to be continuous to a previous one is made to inherit the vertices from it at the point of joining in which case undesirable shapes result not only because of the improper end conditions but probably also because of the uneven subsectioning densities requested on the edges. Proper end conditions may be used as the edges are modelled, however only the first or the second derivative can be made continuous for either one of them but not both may be enforced as end conditions simultaneously. On the other hand, this way, the effect of uneven subsectioning densities will not be a problem anymore. We wish to focus on first order continuity in this case. End conditions may be derived from the given points on the edge, however their computation by fitting quadratics to the last and first three points on the edge did not prove to work satisfactorily for there are usually not enough known points on the edge. The end conditions may also be asked for as part of the input which is adopted in this work. This procedure provides first order continuous modelling always and second order continuous modelling sometimes.

To clarify the points made above, consider two adjacent subregions as in Figure 2.17.

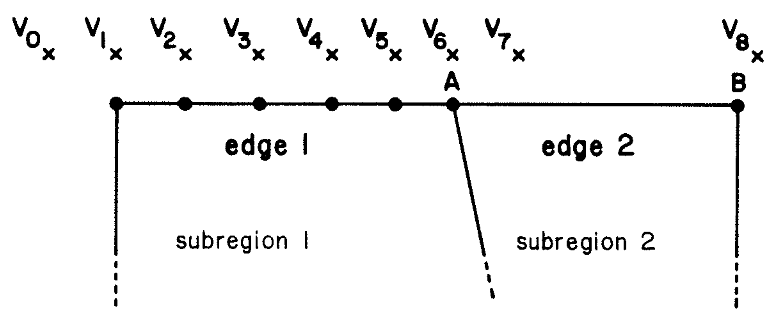

Figure 2.17: Adjacent subregions.

We assume subregion 1 having been processed first and four points generated on its edge 1 with the controlling vertices $V_0, V_1, \ldots, V_7$ determined. The position, the first and the second derivatives at point A are fixed by V_5, V_6 and V_7. If now edge 1 of subregion 2 is to be second order continuous to edge 1 of subregion 1 then the first three vertices of edge 1 of subregion 2 must be V_5, V_6, V_7 leaving V_8 to be determined. Since point B is fixed, the cubic spline model of edge 1 of subregion 2 will assume, in general, an undesirable shape. Continuity of the first derivative, however, can be easily achieved by computing it at A using V_5, V_7 and enforcing this value as the end condition for edge 1 of subregion 2. This way, also the problem of vanishing second derivatives at the interfaces and subregion corners will be eliminated but the "pseudo-flats" will still be present in the model.

Examples and applications of both patch-to-patch discontinuous and continuous modelling are demonstrated in Chapter IV. A different algorithm that does not require end conditions and provides second order continuous modelling is discussed in Chapter V.

Chapter III

BOUNDARY ELEMENT METHOD

In the boundary element model, presented in this Chapter, Laplace's equation to be solved in a volume V is recast into an integral equation that contains the potential and its normal derivative on the surface S which encloses V. The reduction of the integral equation into a set of linear equations is achieved by the Bubnov-Galerkin method with the unknowns and the surfaces represented by bi-cubic spline elements. Also described here are the numerical computation of the principal value integrals and the integration of nearly singular integrands.

3.1 MATHEMATICAL MODEL

Green's second identity is utilized in deriving the boundary integral equation to be solved. From [23, p.252] and [21, p.63], it follows that in a three-dimensional bounded region V with the volume element dV and boundary S which is piecewise smooth, i.e. composed of a finite number of parts each of which including its boundary is continuous and has continuous first derivatives (a regular surface); if ϕ and ψ are two functions of coordinates such that they are continuous, have continuous first derivatives in V+S and piecewise continuous second derivatives in V and if the integrals exist then

$$\int_V (\psi\nabla^2\phi - \phi\nabla^2\psi)\,dv = \int_S (\psi \frac{\partial\phi}{\partial n} - \phi \frac{\partial\psi}{\partial n})\,ds \quad , \tag{3.1}$$

where $\partial/\partial n$ denotes differentiation in the positive direction of the normal. Application of the divergence theorem to the vector $\psi\nabla\phi$ yields Green's first identity

$$\int_V \nabla\psi \cdot \nabla\phi \; dv + \int_V \psi\nabla^2\phi \; dv = \int_S \psi \frac{\partial\phi}{\partial n} \, ds \quad . \tag{3.2}$$

Changing the roles of ψ and ϕ, and subtracting the resulting equation from (3.2) gives (3.1) which is also frequently known as Green's theorem [19, p.165]. It should be noted that the volume V need not be simply-connected [21, p.49].

The validity of (3.1) can be extended to an infinite region V, in which case ϕ and ψ must be regular at infinity, i.e. $R\phi$ and $R\psi$ must be bounded as $R \to \infty$ [21, p.65].

Laplace's equation may be arrived at in different ways. The most direct one in electrostatics seems to be from Maxwell's equations [19, p.160]. In a region V

$$\nabla \times \vec{E} = 0 \quad , \tag{3.3}$$

so that $\vec{E}$ is irrotational and hence conservative. The expression (3.3) is a necessary and sufficient condition for the existence of a potential ϕ in the form

$$\vec{E} = - \nabla\phi \quad . \tag{3.4}$$

Again from Maxwell's equations

$$\nabla \cdot \vec{D} = \rho \qquad (3.5)$$

where ρ is a volume distribution of source density which we assume to be a known and bounded function of position in this work. For a linear and isotropic region of dielectric constant ϵ, the constitutive relation is

$$\vec{D} = \epsilon \vec{E} \quad , \qquad (3.6)$$

and if the region is homogeneous, i.e. ϵ is not a function of position then combining (3.4), (3.5) and (3.6) yields

$$\nabla^2 \phi = -\frac{\rho}{\epsilon} \quad , \qquad (3.7)$$

which is Poisson's equation. In particular, if there are no sources in V

$$\nabla^2 \phi = 0 \quad , \qquad (3.8)$$

which is Laplace's equation.

In order to convert (3.8) into an integral form, we choose a region V enclosed by a surface S where V and S satisfy the conditions of (3.1). Letting $\vec{r}$ and $\vec{r}'$ locate two points in V+S we form the function

$$\psi(\vec{r},\vec{r}') = \frac{1}{|\vec{R}|} \quad , \qquad (3.9)$$

where $\vec{R}=\vec{r}-\vec{r}'$. Except at $\vec{r}=\vec{r}'$, (3.9) is a spherically symmetrical and regular solution of Laplace's equation, i.e.

$$\nabla^2\psi = \nabla'^2\psi = 0 \tag{3.10}$$

in three-dimensional space, and it is known as the fundamental solution or frequently as the free-space Green's function. Its form for two-dimensional space is logarithmic. The expressions of (3.1) and (3.9) for higher dimensional spaces can be found in [23, p.257]. We apply (3.1) to the volume $V-V_\delta$ where V_δ enclosed by S_δ is a sufficiently small sphere of radius δ centered at $\vec{r}'$, as shown in Figure 3.1.

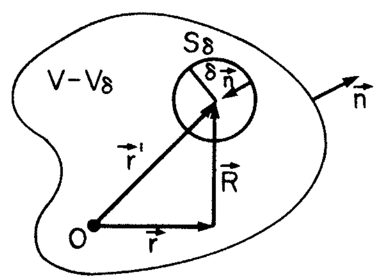

Figure 3.1: Exclusion of the characteristic singularity at $\vec{r}=\vec{r}'$.

Thus (3.1) is written

$$\int_{V-V_\delta} (\psi\nabla^2\phi - \phi\nabla^2\psi)\,dv = \int_{S+S_\delta} (\psi\,\frac{\partial\phi}{\partial n} - \phi\,\frac{\partial\psi}{\partial n})\,ds \tag{3.11}$$

where the coordinates of $\vec{r}$ are the variables of integration and differentiation while those of $\vec{r}'$ locate the observation point. Substituting the values for $\nabla^2\phi$ and $\nabla^2\psi$ from (3.7) and (3.10), respectively, into (3.11) yields

$$-\int_{V-V_\delta} \frac{\rho}{\epsilon R}\,dv = \int_S \left(\frac{1}{R}\frac{\partial\phi}{\partial n} - \phi\frac{\partial}{\partial n}\left(\frac{1}{R}\right)\right)ds + \int_{S_\delta}\left(\frac{1}{R}\frac{\partial\phi}{\partial n} - \phi\frac{\partial}{\partial n}\left(\frac{1}{R}\right)\right)ds \qquad (3.12)$$

where $R=|\vec{R}|$. Over S_δ,

$$\frac{\partial\phi}{\partial n} = -\frac{\partial\phi}{\partial R}\ ,\quad \frac{\partial}{\partial n}\left(\frac{1}{R}\right)\Big|_{R=\delta} = \frac{1}{\delta^2}\ , \qquad (3.13)$$

hence the second integral on the right-hand side of (3.12) is

$$\begin{aligned}\int_{S_\delta}\left(\frac{1}{R}\frac{\partial\phi}{\partial n} - \phi\frac{\partial}{\partial n}\left(\frac{1}{R}\right)\right)ds &= -\frac{1}{\delta}\int_{S_\delta}\frac{\partial\phi}{\partial R}\,ds - \frac{1}{\delta^2}\int_{S_\delta}\phi\,ds \\ &= \left(-\frac{1}{\delta}\overline{\frac{\partial\phi}{\partial R}} - \frac{1}{\delta^2}\bar{\phi}\right)\int_{S_\delta} ds\ ,\end{aligned} \qquad (3.14)$$

where $\partial\bar{\phi}/\partial R$ and $\bar{\phi}$ are some values of $\partial\phi/\partial R$ and ϕ on S_δ. Let $Z(\vec{r}\,')=\int_{S_\delta} dS$, then

$$Z(\vec{r}\,') = \begin{cases} 4\pi\delta^2 & \vec{r}\,' \text{ in } V \\ \Omega\delta^2 & \vec{r}\,' \text{ in } S \\ 0 & \vec{r}\,' \text{ not in } V+S\ , \end{cases} \qquad (3.15)$$

where Ω, as in Figure 3.2, is the conical vertex angle at $\vec{r}\,'$ which is equal to 2π when $\vec{r}\,'$ is on the smooth portion of S [23, p.256].

Now, if $\vec{r}\,'$ is in V and we let $\delta\to 0$ then $\bar{\phi}\to\phi(\vec{r}\,')$ and we obtain

$$\phi(\vec{r}\,') = \frac{1}{4\pi\epsilon}\int_V \frac{\rho}{R}\,dv + \frac{1}{4\pi}\int_S\left(\frac{1}{R}\frac{\partial\phi}{\partial n} - \phi\frac{\partial}{\partial n}\left(\frac{1}{R}\right)\right)ds \qquad (3.16)$$

The convergence of the volume integral in (3.12) when $\delta\to 0$

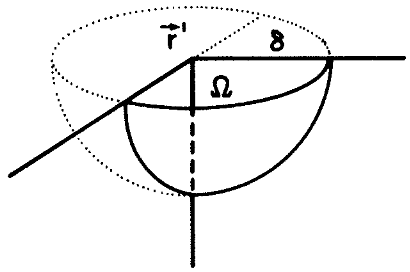

Figure 3.2: Definition of the conical vertex angle.

and of the surface integral in (3.16) is proved in [19, pp.171-189]. The potential at any point in V can be computed by (3.16) if the potential and its normal derivative on S as well as the charge density distribution in V are known. Green's theorem expresses the potential in V as the superposition of potentials due to a volume charge of density distribution ρ, a single layer of charge on S with a density

$$\omega = \epsilon \frac{\partial\phi}{\partial n} \quad , \tag{3.17}$$

and a double layer charge on S of density

$$\tau = \epsilon\,\phi \ . \tag{3.18}$$

If we think of the volume V in (3.16) as a portion of an electrostatic field isolated by the surface S then the single and double layer charges above can be thought of as the sources that account for the effect of the external charges. Hence if there are no sources external to V the surface integral in (3.16) must vanish.

On S, the single layer charge distribution exhibits a discontinuity in the normal derivative of the potential equal to

$$\left.\frac{\partial \phi}{\partial n}\right|_{S^-} - \left.\frac{\partial \phi}{\partial n}\right|_{S^+} = \frac{1}{\epsilon}\,\omega \quad , \tag{3.19}$$

while the double layer charge distribution gives rise to a discontinuity in the potential equal to

$$\phi_{S^-} - \phi_{S^+} = \frac{1}{\epsilon}\,\tau \ . \tag{3.20}$$

By inserting the values of the potential and its normal derivative just inside S into the above discontinuity relationships, we observe that the potential and its normal derivative just outside S are zero. Hence if there are no charges external to S then by (3.16) the field outside S is zero. Therefore, the single layer and the double layer charges in (3.16) are exactly those which reduce the field to zero everywhere external to S [19, p.192].

The Dirichlet problem or the first boundary value problem where

$$\phi = f(s) \text{ on } S \ , \tag{3.21}$$

is given, the Neumann problem or the second boundary value problem in which

$$\frac{\partial \phi}{\partial n} = g(s) \text{ on } S \ , \tag{3.22}$$

is specified and the mixed problem defined with

$$\begin{aligned} \phi &= f(s) \text{ on } S_1 \\ \frac{\partial \phi}{\partial n} &= g(s) \text{ on } S_2 \end{aligned} \qquad S = S_1 + S_2 \ , \tag{3.23}$$

are considered for Laplace's equation. If arbitrary values are assigned to ϕ and $\partial\phi/\partial n$ on S then the potential given by (3.16) is a regular and harmonic function in V but it will not converge to the assigned values of ϕ and its normal derivative on S [21, p.70]. Therefore, (3.16) does not provide a solution to any of the above problems. However when $\vec{r}'$ is on S then

$$\phi(\vec{r}') = \frac{1}{\Omega\epsilon}\int_V \frac{\rho}{R}\, dv + \frac{1}{\Omega}\int_S \left(\frac{1}{R}\frac{\partial \phi}{\partial n} - \phi \frac{\partial}{\partial n}\left(\frac{1}{R}\right)\right) ds \ , \tag{3.24}$$

which constitutes a compatibility condition for ϕ and $\partial\phi/\partial n$ at each point $\vec{r}'$ on S and as such it can be employed to obtain the complementary boundary data in the above problems which can then be substituted in (3.16) to obtain the potential everywhere in V. The expression (3.24) reduces to a Fredholm integral equation of the first kind for $\partial\phi/\partial n$ in the Dirichlet problem, to a Fredholm integral equation of the second kind for ϕ in the Neumann problem and to a combination of the first and second kind Fredholm integral equations in the mixed problem.

It is at this juncture where the simple layer and double layer formulations branch off. A boundary integral equation analogous to (3.16) is stated also for the region exterior to S and the two equations are added. In the resulting expression taking

$$\left.\frac{\partial\phi}{\partial n}\right|_{S^+} - \left.\frac{\partial\phi}{\partial n}\right|_{S^-} = 0$$

$$\frac{\mu(s)}{\epsilon} = \phi_{S^-} - \phi_{S^+} \tag{3.25}$$

leads to the double layer formulation while choosing

$$\phi_{S^+} - \phi_{S^-} = 0$$

$$\frac{\sigma(s)}{\epsilon} = \left.\frac{\partial\phi}{\partial n}\right|_{S^+} - \left.\frac{\partial\phi}{\partial n}\right|_{S^-} , \tag{3.26}$$

yields the simple layer formulation [38], [51].

The existence and uniqueness of solutions for the interior and exterior Dirichlet problems with the Green's theorem formulation are proved in [24,ch.3]. The uniqueness, except for an arbitrary added constant , and existence of the solution for the interior Neumann problem requires that

$$\oint_S \frac{\partial\phi}{\partial n}\, ds = 0 \quad , \tag{3.27}$$

while for the exterior, where the condition (3.27) is not necessarily satisfied, the solution exists and is unique [21, p.292]. For the mixed problem, existence and uniqueness of solutions are proved in [25], [26].

The region of interest for the solution of Laplace's equation consists of piecewise homogeneous media in this work. Green's theorem is applied to each homogeneous medium with the following conditions that are valid at the media interfaces. The normals are out of the respective media.

$$\phi_1 = \phi_2$$

$$\epsilon_1 \frac{\partial\phi}{\partial n_1} + \epsilon_2 \frac{\partial\phi}{\partial n_2} = 0 \ . \tag{3.28}$$

The existence and uniqueness of solutions for a system of dielectrics are given in [24, p.254], [19, pp.194-197].

3.2 THE GALERKIN METHOD

After the physical problem is reduced to a mathematical model which satisfies the requirements of existence, uniqueness and continuous dependence on data, a proper numerical technique has to be adopted for the solution. If the mathematical model is based on partial differential equations the numerical methods will entail approximations to be made throughout the region of the problem while approximations are done only on the boundary if the problem is formulated through boundary integral equations. Thus the first distinction among various methods is the mathematical model which they solve. Since the dimensionality of the problem is reduced by one, the boundary integral equation formulations are desirable. The Bubnov-Galerkin method, which is explained below, is employed in this work.

The Galerkin method is a particular one of the projection methods [34, p.253], [36], which are also termed as methods of weighted residuals [31]. The idea of projection methods is as follows. Consider the inhomogeneous equation

$$L\,x = f \quad , \tag{3.29}$$

where f is known, x is to be determined and L is an operator which maps from the space X to the space F with the domain $D(L) \subseteq X$ and the range $R(L) \subseteq F$. Assume that $\{X_n\}$ and $\{F_n\}$ are two given sequences of subspaces with

$$X_n \subseteq D(L) \ , \ F_n \subseteq F \quad (n = 1,2,\ldots) \quad , \tag{3.30}$$

and P_n are the projection operators from F to F_n as

$$P_n^2 = P_n \ , \ P_n F = F_n \quad (n=1,2,\dots) \ . \tag{3.31}$$

The method seeks a solution x_n to (3.29) through the approximation

$$P_n(L\, x_n - f) = 0 \ , \ x_n \in X_n \ . \tag{3.32}$$

The case when X=F, $X_n = F_n$ (n=1,2,...) is the Galerkin method. The construction of subspaces X_n, F_n and the operators P_n form the basis of the projection methods. The cases when X and F are Banach spaces or when L is nonlinear are investigated with regards to the existence, uniqueness and convergence of solutions in [36].

The domain of the operator in the integral equations of this work is the space of all square-integrable functions on the boundary S, i.e. $L_2(S)$ which is a Hilbert space with the inner product

$$\langle g,h \rangle_2 = \int_S g(s)h(s)ds \ ; \ g,h \in L_2(S) \tag{3.33}$$

and the norm

$$\|g\|_2 = \langle g,g \rangle_2^{1/2} \ . \tag{3.34}$$

It is worth noting that since the kernels of the integrals in (3.24) are of the form

$$K(\vec{r},\vec{r}\,') = \frac{A(\vec{r},\vec{r}\,')}{|\vec{r}-\vec{r}\,'|^{\alpha}} \ , \ 0 < \alpha < 2 \tag{3.35}$$

i.e. weakly singular, initially they may not seem to be square-integrable. However, the order of the singularity is shown to be $\alpha=1$ when $\vec{r}\to\vec{r}\,'$ [27, p.113], hence the kernel remains square-integrable and the operator is completely continuous [24, p.21], [34, p.270].

When L is linear, bounded and completely continuous and X and F are Hilbert spaces, the subspaces X_n, F_n and the projections P_n are constructed as follows. We select two sets of finite number, linearly independent coordinate functions $\{w_i\}_{i=1}^{n}$ in X and $\{f_i\}_{i=1}^{n}$ in F. Then

$$
\begin{aligned}
X_n &= \mathrm{span}\ \{w_i\}_{i=1}^{n} \\
F_n &= \mathrm{span}\ \{f_i\}_{i=1}^{n} \quad ,
\end{aligned}
\tag{3.36}
$$

and since $x_n \in X_n$

$$
x_n = \sum_{i=1}^{n} a_i\, w_i \quad , \tag{3.37}
$$

where the coefficients a_i are determined by the condition that the residual $E=Lx_n-f$ be orthogonal to $\{f_i\}_{i=1}^{n}$, i.e.

$$
\langle Lx_n - f, f_i \rangle = 0 \quad , \tag{3.38}
$$

which gives a linear system of equations for a_i,

$$
\sum_{j=1}^{n} \langle Lw_j, f_i \rangle a_i = \langle f, f_i \rangle \qquad (i=1,2,\ldots,n) \quad . \tag{3.39}
$$

This is the Galerkin-Petrov method. Here the coordinate functions are finite in number, P_n is the orthogonal projection and $X_n \subset X_{n+1}$, $F_n \subset F_{n+1}$.

When the elements f_i are chosen as

$$f_i = Lw_i \quad (i=1,2,\ldots,) \quad , \tag{3.40}$$

the method subsumes the least-squares method [39]. The method of moments [37] and the collocation method can be shown to be included in the projection methods.

The variant of the Galerkin-Petrov method in which E=F and the coordinate sequences coincide ($w_i = f_i$) is known as the Bubnov-Galerkin method.

At this juncture it is natural to ask if there exists a solution to the Galerkin equations and if it does then whether it is unique. We further wish to know if the numerical result will converge to the exact solution as the dimension of the approximation space is increased. The convergence here is to be interpreted as a compensating argument since the projection method is not an iterative method in the sense that x_n is determined using previous approximations $x_1, \ldots, x_{n-1}$.

The Rayleigh-Ritz variational method, which can be constructed if a functional for the variational problem is known, is shown to provide a solution if the operator is self-adjoint and the solution is known to be unique if the operator is positive-definite, and to converge to the exact solution if the operator is positive-bounded-below [32]. Since the Rayleigh-Ritz equations are also known to be identical to the Bubnov-Galerkin equations one argues that if the operator satisfies the above conditions then whether the problem is formulated via the Rayleigh-Ritz method or the Bubnov-Galerkin method we have the existence, uniqueness and convergence guarantees for the solution. However, we know that the Galerkin method can be applied to nonlinear, non-self-adjoint or non-positive-definite operator equations as well. It is shown that integral equations with nonsymmetric kernels corresponding to non-self-adjoint operator equations can be converted to self-adjoint forms by making the kernels symmetric [40, p.908],[22, p.159], [41], however non-positive-definite kernels can be brought only to positive-semidefinite forms in general in which case not much can be concluded about uniqueness and convergence. Nevertheless, less stringent sufficient conditions than those above, for the existence, uniqueness and convergence of the Bubnov-Galerkin solutions, have been shown to exist. A theorem due to Mikhlin [34, p.250] which requires only linearity of the operator states that if L can be split up as $L=L_0+L_1$ where L_0 is self-adjoint, positive-bounded-below in a given Hilbert space H and L_1 is completely continuous (compact) in the energy space H_{L_0} such that $D(L_1)\supset D(L_0)$ and the sequence of subspaces $\{X_n\}$ is ultimately dense in $D(L_0)$, i.e. the coordinate functions possess the approximation property [44] or the coordinate functions are members of $D(L_0)$ and form a complete set in H_{L_0} then for sufficiently large n, the Bubnov-Galerkin system of equations have a unique solution that converges to the exact solution in the norm of H_{L_0} or in the metric of H [34, p.293]. An estimate for the convergence is given by

$$\|x - x_n\|_2 \leq (1 + \epsilon_n) \|x - P_n x\| \quad , \tag{3.41}$$

where $\epsilon_n \to 0$ as $n \to \infty$.

Strongly elliptic systems [25] are known to satisfy the Garding inequality [8], which then implies that the operator L can be decomposed exactly as required in the above theorem [44]. Among the strongly elliptic operator equations are the Fredholm's first and second kind equations with weakly singular kernels arising in electrostatics [44]. Moreover, the finite element functions as well as splines when used as coordinate functions have been shown to satisfy the approximation property [8, p.269], [44]. In view of the above, the Bubnov-Galerkin method as used in this work yields a solution that is unique and converges in the mean to the exact solution as the dimension of the approximation space is increased. It is further known that, in fact, strong ellipticity is necessary for the convergence of all Galerkin methods due to Vainikko [44].

3.3 NUMERICAL FORMULATION

Consider a problem with piecewise homogeneous media as in Figure 3.3 where $e_{i,m}$ is the m-th element in the i-th region.

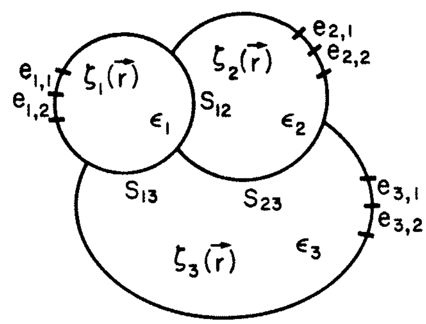

Figure 3.3: A multi-media configuration.

In general there may be any number of regions with boundaries S_i. The interfaces are denoted by S_{ij}. The S_i encloses the connected region V_i, $i=1,2,\ldots,N$ where N is the total number of regions each of which is homogeneous with material property ϵ_i and may contain volume sources of given density $\rho_i(\vec{r})$. In this work only $\rho_i(\vec{r})$ in the form of discrete point sources is considered.

With respect to Figure 3.4, writing (3.24) explicitly in

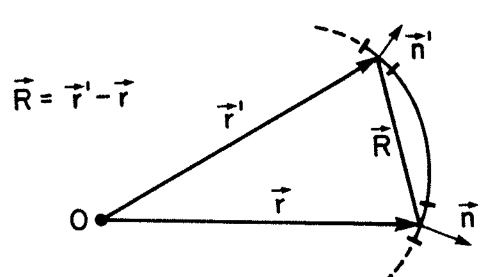

Figure 3.4: Notations for the boundary integral equation.

Cartesian coordinate system yields

$$\begin{aligned}\phi(x',y',z') &= \frac{1}{2\pi\epsilon}\int_V \frac{\rho(x,y,z)}{R(x',y',z';x,y,z)}\,dv(x,y,z) \\ &+ \frac{1}{2\pi}\int_S \frac{1}{R(x',y',z';x,y,z)}\,\frac{\partial\phi(x,y,z)}{\partial n(x,y,z)}\,ds(x,y,z) \\ &- \frac{1}{2\pi}\int_S \phi(x,y,z)\,\frac{\partial}{\partial n(x,y,z)}\left(\frac{1}{R(x',y',z';x,y,z)}\right)ds(x,y,z)\quad ,\end{aligned} \tag{3.42}$$

where we assume S to be smooth and

$$R(x',y',z';x,y,z) = [(x'-x)^2 + (y'-y)^2 + (z'-z)^2]^{\frac{1}{2}} \tag{3.43}$$

$$\frac{\partial}{\partial n(x,y,z)}\left(\frac{1}{R}\right) = \nabla\left(\frac{1}{R}\right)\cdot\vec{n} = \frac{1}{R^3}\{(x'-x)\vec{a}_x + (y'-y)\vec{a}_y + (z'-z)\vec{a}_z\}\cdot\vec{n} \quad . \tag{3.44}$$

The equation (3.42) is discretized for each region and the resulting equations are solved simultaneously for the unknown potential or normal derivative of the potential on the boundary and at the interfaces. We will focus on the discretization of (3.42) for a single region first and later we will show how the coupled equations are solved if there is more than one region. We express the potential and its normal derivative on the surface with a set of expansion functions denoted by $\{w_i\}_{i=1}^{n}$, i.e.

$$\begin{aligned}\phi_S &= \sum_{i=1}^{n} \phi_i\, w_i \\ \left.\frac{\partial\phi}{\partial n}\right|_S &= \sum_{i=1}^{n} \left(\frac{\partial\phi}{\partial n}\right)_i w_i \quad ,\end{aligned} \tag{3.45}$$

where the coefficients are either known or to be determined.

Thus (3.42) becomes

$$\sum_{i=1}^{n} w_i\phi_i + \frac{1}{2\pi}\int_S \sum_{i=1}^{n} w_i\phi_i \frac{\partial}{\partial n}\left(\frac{1}{R}\right)ds = \frac{1}{2\pi}\int_S \sum_{i=1}^{n} w_i\left(\frac{\partial\phi}{\partial n}\right)_i \frac{1}{R}\,ds + q \quad , \tag{3.46}$$

where q is the volume integral of the point sources of value s_j and located at u_j, i.e.

$$q = \frac{1}{2\pi\epsilon}\int_V \sum_{j=1}^{m} \frac{s_j\delta(\vec{u}_j-\vec{r})}{R(\vec{r},\vec{r}\,')}\,dv = \frac{1}{2\pi\epsilon}\sum_{j=1}^{m} \frac{s_j}{R(\vec{u}_j,\vec{r}\,')} \quad . \tag{3.47}$$

Application of the Bubnov-Galerkin method yields

$$\begin{aligned}\int_S w_j\left(\sum_{i=1}^{n} w_i\phi_i\right)ds' + \int_S w_j\left(\frac{1}{2\pi}\int_S \sum_{i=1}^{n} w_i\,\phi_i \frac{\partial}{\partial n}\left(\frac{1}{R}\right)ds\right)ds' \\ = \int_S w_j\left(\frac{1}{2\pi}\int_S \sum_{i=1}^{n} w_i\left(\frac{\partial\phi}{\partial n}\right)_i \frac{1}{R}\,ds\right)ds' + \int_S w_j\,q\,ds' \qquad (j=1,\dots,n)\end{aligned} \tag{3.48}$$

for which the matrix form is

$$[F]\underline{\phi} = [H]\,\underline{\frac{\partial\phi}{\partial n}} + \underline{Q} \quad , \tag{3.49}$$

In the Dirichlet problem $\partial\phi/\partial n$ and in the Neumann problem ϕ is solved for while in the mixed problem a combination of ϕ and $\partial\phi/\partial n$ has to be computed from (3.49). Thus depending on the problem (3.49) is brought into the form

$$[S]\underline{\lambda} = \underline{b} \quad , \tag{3.50}$$

and solved. Since both the potential and its normal derivative are expanded with the same set of basis functions, if at a point on the boundary neither ϕ nor $\partial\phi/\partial n$ is known then the coefficient matrix in (3.50) will be singular. Therefore at any point on the boundary either ϕ or $\partial\phi/\partial n$ must be given and wherever both are specified they must be compatible.

To compute the matrix entries we consider

$$S = \bigcup_{i=1}^{m} e_i \quad , \tag{3.51}$$

where the elements e_i are non-overlapping. From (3.48) and (3.51), it is readily seen that the coefficient matrices can be generated easily in an element by element fashion.

The product form of Gauss-Legendre quadrature is used for the integrations [45]. This scheme, unlike the Newton-Cotes integration formulae, guarantee convergence when the quadrature order is increased [62, p.267]. The rule in ξ, η system of coordinates is

$$\int_0^1\int_0^1 f(\xi,\eta)\,d\xi\,d\eta = \sum_{j=1}^{m} a_j\left(\sum_{i=1}^{n} a_i\; g(\nu_i,\nu_j)\right) \tag{3.52}$$

where

$$\begin{aligned} g(\nu_i,\nu_j) &= \frac{1}{2}\cdot\frac{1}{2}\cdot f(\xi,\eta) \\ \xi &= \frac{1}{2}\,\nu_i + \frac{1}{2} \\ \eta &= \frac{1}{2}\,\nu_j + \frac{1}{2} \quad . \end{aligned} \tag{3.53}$$

The a's and ν's , called weights and abcissas respectively, are to be found in [45]. It is known that n point Gauss-Legendre quadrature integrates polynomials of degree 2n-1 exactly [5]. Thus each $\int_e f(x,y,z)\;dS$ must be transformed to $\int_0^1\int_0^1 g(\xi,\eta)\;d\xi d\eta$ which is done using standard bi-variate finite elements. This work employed bi-cubic spline elements and defined the element geometries by

$$x = \sum_{i=1}^{12} x_i \, A_i(\xi,\eta)$$
$$y = \sum_{i=1}^{12} y_i \, A_i(\xi,\eta) \qquad (3.54)$$
$$z = \sum_{i=1}^{12} z_i \, A_i(\xi,\eta) \quad ,$$

in which case the unit surface normal is

$$\vec{n} = \frac{1}{J}\left(\frac{\partial(y,z)}{\partial(\xi,\eta)}\,\vec{a}_x + \frac{\partial(z,x)}{\partial(\xi,\eta)}\,\vec{a}_y + \frac{\partial(x,y)}{\partial(\xi,\eta)}\,\vec{a}_y\right) , \qquad (3.55)$$

and the Jacobian of the transformation is

$$J = \left[\frac{\partial(y,z)}{\partial(\xi,\eta)}^2 + \frac{\partial(z,x)}{\partial(\xi,\eta)}^2 + \frac{\partial(x,y)}{\partial(\xi,\eta)}^2\right]^{\frac{1}{2}} \qquad (3.56)$$

where the partial derivatives are obtained analytically by differentiating the shape functions.

As regards the unknowns, the relation between the global w_i and local W_i is as follows. Each w_i is associated with a point which is a vertex of e_j or a midside node and is shared among a number of elements. That portion of w_i which lies in e_j corresponds to W_ℓ when e_j is transformed to $[0,1]\times[0,1]$. The picture is clearer when Figure 3.5 is considered which shows the correspondence in two dimensions.

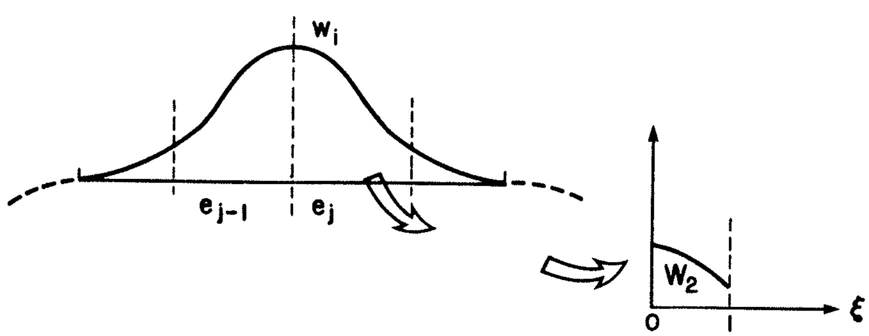

Figure 3.5: Correspondence between global w_i and local W_i.

In particular, when $W_i = A_i$, i.e. the unknowns and the geometry are expressed with the same expansion function, we have an isoparametric method; when geometry is modelled with less number of parameters than the unknowns a subparametric method results and when the geometry is defined with more number of parameters than the unknowns a superparametric method is obtained [4, p.123].

In the program implementation an isoparametric method with bi-cubic spline elements is adopted and for the integrals the same number of Gauss-Legendre quadrature points is used in both directions.

<u>Principal Value Integrations</u>

There are two cases in which the kernels in (3.24) are unbounded though their integrals exist in the principle value sense. One situation arises when the normal derivative of the potential becomes infinite which usually happens at points on the boundary with conical vertex angles greater than 2π [24, p.164], [6]. No attempt has been made, in this work, to model the unbounded $\partial\phi/\partial n$'s with the proper form imposed on the expansion functions [50], however the second situation which occurs when $1/R$ and $\partial/\partial n(1/R)$ become infinite as $\vec{r}=\vec{r}\,'$ is appropriately catered to.

The field and source points coincide, i.e. $\vec{r}=\vec{r}\,'$, at the matrix set up process in the terms

$$\int_{e_i} w_i \int_{e_i} \sum_{i=1}^{n} w_i \, \phi_i \frac{\partial}{\partial n}\left(\frac{1}{R}\right) ds \; ds' \, , \quad \int_{e_i} w_i \int_{e_i} \sum_{i=1}^{n} w_i \frac{1}{R} \left(\frac{\partial \phi}{\partial n}\right)_i ds \; ds' \, , \qquad (3.57)$$

and also whenever the potential at a point on the surface is to be computed. The integrals when $\vec{r}=\vec{r}'$ are known to exist, however they pose great difficulty for numerical computation. The tricks of skipping the singularity or avoiding it by employing different orders of quadrature for the inner and outer integrals and other methods have been shown not to work satisfactorily [49]. The method we employ here, which follows from [46], [49], and is the same as in [50], aims at eliminating the singularity and converting the integrand to a well-behaved form that is amenable to computer evaluation.

In this method, whenever $\vec{r}=\vec{r}'$ occurs the unit square is divided into four triangles about the local coordinates of $\vec{r}'$ which we shall show by (a,b). The value of the integral is found by evaluating it on each triangle separately and adding the results. The process is shown in Figure 3.6.

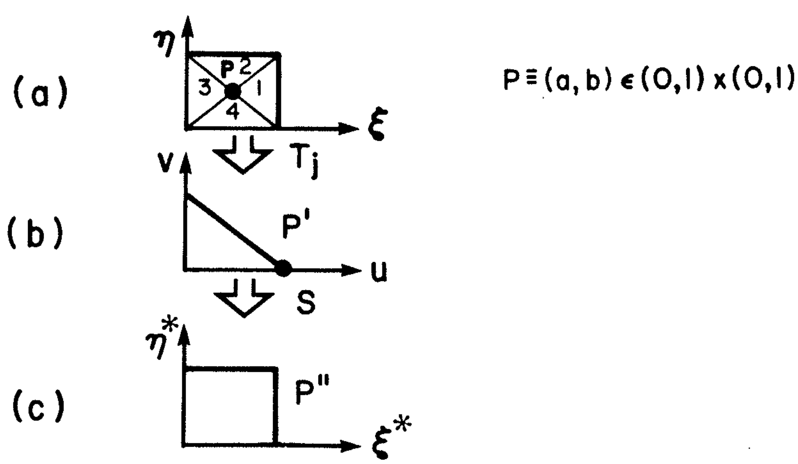

Figure 3.6: Catering to kernel singularities.

Consider the integral

$$I = \int_0^1 \int_0^1 f(\xi,\eta)\, d\xi\, d\eta \tag{3.58}$$

where $f(\xi,\eta)$ has an isolated singularity that is a pole of order one at (a,b). The integral is split up on four triangles as follows.

$$\begin{aligned} I = &\int_a^1 \int_{\frac{b}{a-1}(\xi-1)}^{\frac{1-b}{1-a}(\xi-1)+1} f(\xi,\eta)\, d\eta\, d\xi + \int_b^1 \int_{\frac{a}{b-1}(\eta-1)}^{\frac{1-a}{1-b}(\eta-1)+1} f(\xi,\eta)\, d\xi\, d\eta \\ &+ \int_0^a \int_{\frac{b}{a}\xi}^{\frac{b-1}{a}\xi+1} f(\xi,\eta)\, d\eta\, d\xi + \int_0^b \int_{\frac{a}{b}\eta}^{\frac{a-1}{b}\eta+1} f(\xi,\eta)\, d\xi\, d\eta \end{aligned} \tag{3.59}$$

The first, second, third and fourth integrals of (3.59) are transformed by T_1, T_2, T_3 and T_4 respectively to integrals on a simplex of the form (b) where

$$T_1:\quad \begin{aligned} \xi &= (a-1)u + 1 \\ \eta &= (b-1)u - v + 1 \\ J &= (1-a) \end{aligned} \tag{3.60}$$

$$T_4:\quad \begin{aligned} \xi &= (a-1)u - v + 1 \\ \eta &= bu \\ J &= -b \end{aligned} \tag{3.61}$$

$$T_2:\quad \begin{aligned} \xi &= au + v \\ \eta &= (b-1)u + 1 \\ J &= (b-1) \end{aligned} \tag{3.62}$$

$$T_3:\quad \begin{aligned} \xi &= au \\ \eta &= bu + v \\ J &= a \end{aligned} \tag{3.63}$$

such that P maps to P'. Thus (3.59) becomes

$$
\begin{aligned}
I = & \int_0^1 \int_0^{1-u} f\Big((a-1)u+1,(b-1)u-v+1\Big)(1-a)\,dv\,du \\
& + \int_0^1 \int_0^{1-u} f\Big(au+v,(b-1)u+1\Big)(1-b)\,dv\,du \\
& + \int_0^1 \int_0^{1-u} f(au,bu+v)a\,dv\,du \\
& + \int_0^1 \int_0^{1-u} f\Big((a-1)u-v+1,bu\Big)b\,dv\,du \quad ,
\end{aligned}
\tag{3.64}
$$

with the respective integrals. Next, (3.64) is transformed by

$$
\begin{aligned}
S\ :\ \ u &= \xi^* \\
v &= \eta^*(1-\xi^*) \\
J &= 1-\xi^* \quad ,
\end{aligned}
\tag{3.65}
$$

to the unit square in (c). Note that the singularity point P' maps to the collapsed edge here. Hence (3.64) becomes

$$
\begin{aligned}
I = \int_0^1\int_0^1 \Big\{ & f\Big((a-1)\xi^*+1,(b-1)\xi^*-\eta^*(1-\xi^*)+1\Big)(1-a) \\
& + f\Big(a\xi^*+\eta^*(1-\xi^*),(b-1)\xi^*+1\Big)(1-b) \\
& + f\Big(a\xi^*,b\xi^*+\eta^*(1-\xi^*)\Big)a \\
& + f\Big((a-1)\xi^*-\eta^*(1-\xi^*)+1,b\xi^*\Big)b\Big\}(1-\xi^*)\,d\eta^*\,d\xi^* \quad ,
\end{aligned}
\tag{3.66}
$$

which can be integrated numerically with

$$
I \approx \sum_{i=1}^{n} a_i(1-\nu_i)\left\{\sum_{i=1}^{n} a_j\, F(\nu_i,\nu_j)\right\} \ . \tag{3.67}
$$

In (3.66), we observe that when $\xi^* \to 1$, i.e approaching the collapsed edge, $(1-\xi^*) \to 0$ and $F(\xi^*,\eta^*) \to 2f(a,b)$. Thus

$$
\lim_{\xi^* \to 1} F(\xi^*,\eta^*)\ (1-\xi^*) = 0(1) \quad , \tag{3.68}
$$

which is a bounded and well-behaved integrand. Since the term $\partial/\partial n(1/R)$ approaches $1/R$ in the limit as $\vec{r}=\vec{r}'$, the treatment of $1/R$ applies also to the case of $\partial/\partial n(1/R)$.

<u>Nearly Singular Integrands</u>

An important problem, which arises when $\vec{r}+\vec{\epsilon}=\vec{r}'$ where $\vec{\epsilon}$ is very small, results in degraded accuracy in the numerical integrations if not handled properly. The problem, firstly, occurs for adjacent elements at the matrix set up step, as illustrated in a two-dimensional cross section in Figure 3.7. The integral corresponding to the term $\partial/\partial n(1/R)$ may vanish when both elements are on the same plane, or may cause a more severe problem than that of $1/R$ when the interface between the elements happens to be an edge.

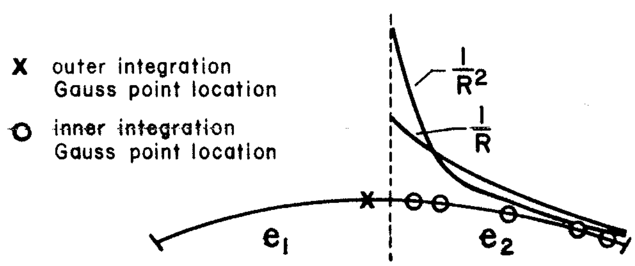

Figure 3.7: Adjacent boundary elements.

The problem, secondly, occurs when the point where the potential is to be computed is very close to the boundary as shown in Figure 3.8.

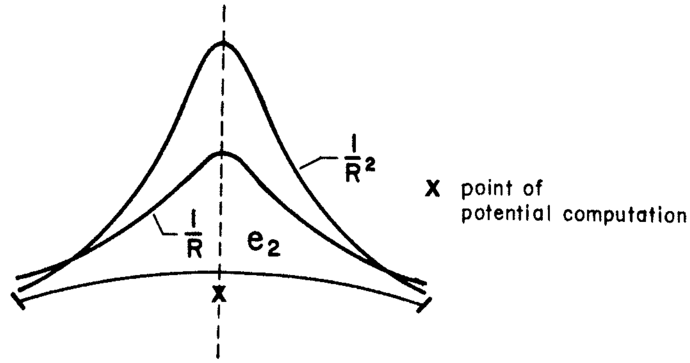

Figure 3.8: Point very close to the boundary.

The adaptive method, we employ here, first determines if the integrals can be computed accurate enough with the given quadrature order and if not divides the element into a number of subelements and adds the integrals, computed on each subelement separately, to obtain the result. The advantage here as opposed to using a higher order Gaussian quadrature is that this method and the method of principal value integration can share the same computer storage since either $\vec{r}=\vec{r}\,'$ or $\vec{r}+\vec{\epsilon}=\vec{r}\,'$ is the case but not both. The procedure is shown in Figure 3.9.

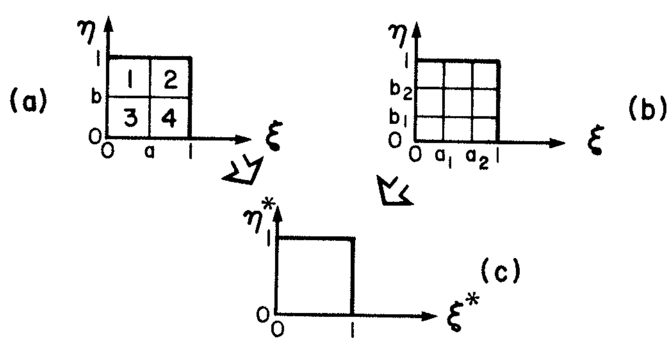

Figure 3.9: Catering to nearly singular integrands.

Consider the integral

$$I = \int_0^1\int_0^1 f(\xi,\eta)\,d\xi\,d\eta \tag{3.69}$$

It is split up on four subelements about the point (a,b)

$$I = \int_b^1\int_0^a f(\xi,\eta)\,d\xi\,d\eta + \int_b^1\int_a^1 f(\xi,\eta)\,d\xi\,d\eta + \int_0^b\int_0^a f(\xi,\eta)\,d\xi\,d\eta + \int_0^b\int_a^1 f(\xi,\eta)\,d\xi\,d\eta\ . \tag{3.70}$$

The integrals in (3.70) are then transformed to (c) by

$$\begin{aligned}
&T_1:\ \xi = a\xi^* &&,\quad \eta = (1-b)\eta^* + b &&,\quad J = a(1-b)\\
&T_2:\ \xi = (1-a)\xi^* + a &&,\quad \eta = (1-b)\eta^* + b &&,\quad J = (1-a)(1-b)\\
&T_3:\ \xi = a\xi^* &&,\quad \eta = b\eta^* &&,\quad J = ab\\
&T_4:\ \xi = (1-a)\xi^* + a &&,\quad \eta = b\eta^* &&,\quad J = (1-a)b\ ,
\end{aligned} \tag{3.71}$$

respectively and (3.70) becomes

$$\begin{aligned}
I = \int_0^1\int_0^1 \{&f(a\xi^*,(1-b)\eta^*+b)a(1-b) + f((1-a)\xi^*+a),(1-b)\eta^*+b)(1-a)(1-b)\\
&+ f(a\xi^*,b\eta^*)ab + f((1-a)\xi^*+a,b\eta^*)(1-a)b\}d\xi^*\,d\eta^*\ .
\end{aligned} \tag{3.72}$$

Subdivision of the unit square into more subelements, e.g. into nine subelements as shown in Figure 3.9, follows similarly.

Analysis of Errors

The accuracy of the numerical results depends on the errors committed with regards to the following points.

i. the modelling of the problem geometry,

ii. the number of expansion functions,

iii. the modelling of the unknowns,

iv. the numerical integrations,

v. the word length of the computer.

An error analysis which aims at calculating the effects of the above points to the total error has not been pursued. Instead the following procedure has been considered to be useful in determining the accuracy of a candidate solution. If there exists a maximum principle for the problem then since the computed potential $\tilde{\phi}$ and the exact potential ϕ are both harmonic so will be the error $E=|\phi-\tilde{\phi}|$ and attain its maximum value on the boundary. This to be an effective error bound $\tilde{\phi}$ must be computed at a large number of points on the boundary. If a maximum principle is not available results for increasing number of elements can be computed and compared with each other. Comparison of the numerical results against exact solutions for analytically solvable problems is a clear indication of the achievable accuracies with the method. Such problems are demonstrated in the next Chapter.

Chapter IV

APPLICATIONS

This Chapter includes several applications of the data preparation method and the boundary element method. The data preparation applications involve two-dimensional finite element generation and three-dimensional boundary element generation while the examples regarding the boundary element method aim at demonstrating the accuracies achievable with the method and as such they include comparisons between computed and exact results for analytically solvable problems. Both methods are programmed in FORTRAN IV and ran on the AMDAHL 470/V8 computer of the University of Manitoba. The boundary element method results are obtained in double precision arithmetic.

In the examples, the following error definitions are used. On an interval [a,b], to express the distance (absolute error, E_a) between the exact function f(x) and its approximation $\tilde{f}(x)$ we use the metric $d(f,\tilde{f})$ which is induced either by the Tchebycheff norm, i.e.

$$E_{a,T} = d(f,\tilde{f}) = \|f(x) - \tilde{f}(x)\|_T = \max_{a \le x \le b} |f(x) - \tilde{f}(x)| , \qquad (4.1)$$

or by the L_1 norm [29, p.62], i.e.

$$E_{a,1} = d(f,\tilde{f}) = \|f(x) - \tilde{f}(x)\|_1 = \int_a^b |f(x) - \tilde{f}(x)| dx . \qquad (4.2)$$

The L_2 norm is not preferred here for it is a much weaker measure of good approximation than the Tchebycheff and L_1 norms [8, p.10]. It is usually more desirable to know the distance between f(x) and $\tilde{f}(x)$ relative to some length (relative error, E_r). In this case we choose this length to be the norm of the exact function and define

$$E_{r,T} = \frac{\max_{a\le x\le b} |f(x) - \tilde{f}(x)|}{\max_{a\le x\le b} |f(x)|} * 100\% \quad , \tag{4.3}$$

$$E_{r,1} = \frac{\int_a^b |f(x) - \tilde{f}(x)|dx}{\int_a^b |f(x)|dx} * 100\% \quad . \tag{4.4}$$

Often it is not feasible to work on the continuous interval [a,b] but on set of equally spaced points P_m: $a=x_1<x_2<...<x_m=b$. We then define

$$\tilde{E}_{a,T} = \max_{x\in P_m} |f(x) - \tilde{f}(x)| \tag{4.5}$$

$$\tilde{E}_{a,1} = \frac{a-b}{m} \sum_{i=1}^{m} |f(x_i) - \tilde{f}(x_i)| \tag{4.6}$$

$$\tilde{E}_{r,T} = \frac{\max_{x\in P_n} |f(x) - \tilde{f}(x)|}{\max_{a\le x\le b} |f(x)|} * 100\% \tag{4.7}$$

$$\tilde{E}_{r,1} = \frac{(a-b)\sum_{i=1}^{m} |f(x_i) - \tilde{f}(x_i)|}{m \cdot \int_a^b |f(x)|dx} * 100\% \tag{4.8}$$

and if the norm of f(x) is not available then we substitute the norm of $\tilde{f}(x)$ in (4.7) and (4.8). The Tchebycheff norm may be thought of as the worst case error while the L_1 norm may be interpreted as an average error.

4.1 DATA PREPARATION EXAMPLES

The first test demonstrates the accuracy of approximating functions with cubic B-splines. The unit circle, r=1, is approximated with increasing number of data points first by a closed cubic spline hence second order continuous (case 1) and second, by four natural cubic spline segments of equal length (case 2). The errors in percentage are shown in Table 4.1.

TABLE 4.1

Accuracy of cubic spline approximation of unit circle

number of points	case 1		case 2	
	$E_{r,T}$	$E_{r,1}$	$E_{r,T}$	$E_{r,1}$
4	2.77	1.44	29.3	18.8
8	0.115	0.0610	2.97	1.66
12	0.0210	0.0112	1.39	0.683
16	0.00647	0.00345	0.762	0.276
20	0.00262	0.00139	0.488	0.157

Clearly, for a given number of data points the closed cubic spline fit yields a more accurate approximation for the circle and the accuracy increases as more data points are taken. The approximations with 8 data points for case 1 and case 2 are shown in Figure 4.1.

The unit sphere, r=1, is modelled with 8 Coons patches, one per octant. The patch boundaries are made up of segments of the three unit circles that lie in the x-y, y-z and z-x

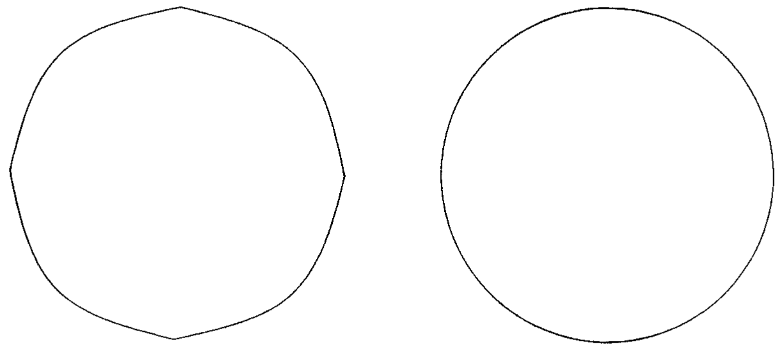

Figure 4.1: Cubic spline models for the unit circle with 8 points.

planes which are modelled as above in case 1 and case 2, with increasing accuracy. The errors in percentage are given in Table 4.2 where the first column refers to the number of data points on the circles.

TABLE 4.2

Accuracy of the Coons patch model for the unit sphere

number of points	case 1		case 2	
	$E_{r,T}$	$E_{r,1}$	$E_{r,T}$	$E_{r,1}$
4	7.76	2.67	42.2	26.5
8	5.00	0.799	6.25	2.96
12	4.94	0.747	4.60	1.35
16	4.96	0.747	4.84	0.978
∞	4.96	0.745	----	----

From Table 4.2,it is seen that up to a point the accuracy of the Coons patch model increases as the boundary curves become more accurate and when the boundary curves are exact the error reaches a limit which may be reduced further if more Coons patches are taken. The absolute errors for the unit circle and the unit sphere may be obtained through dividing the above relative errors by 100.

Finite Element Generation

An example of the finite element mesh generation and data preparation method is furnished by the modelling of an electrical machine rotor crossection. Figure 4.2 depicts the region to be discretized.

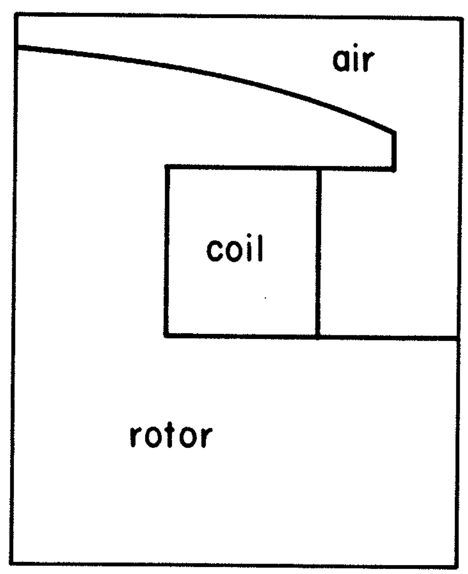

Figure 4.2: One-half pole pitch rotor crossection.

In order to have the most flexibility in data modification and editing the region has been divided into 14 subregions (Coons patches). The program [59], automatically, discretized the region into elements and prepared the geometrical description data. Figure 4.3 shows the finite element mesh.

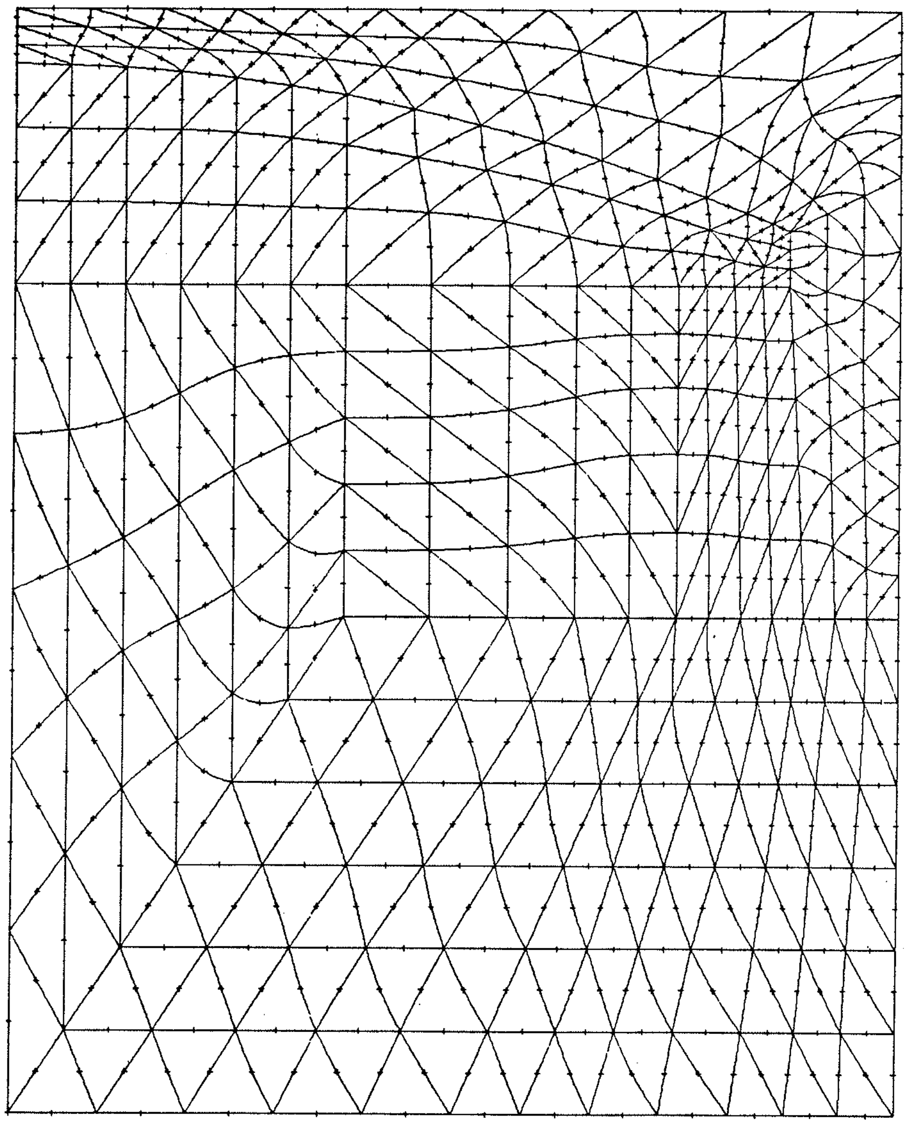

Figure 4.3: Finite element model of the rotor crossection.

The geometrical description data for the problem may be interfaced to MANFEP [56] at which step the boundary conditions, material properties and finite element program parameters are defined.

The data preparation program [55] has been used extensively in many practical problems with complex geometries as well as in research oriented applications [57], [58], [60], [61], [63].

Boundary Element Generation

The method is capable of generating triangular and quadrilateral Lagrangian elements as well as cubic spline elements of Chapter II on surfaces. Plotting and interfacing programs have been developed to display the boundary elements and to transform the geometrical description data to the particular field analysis program. Figure 4.4 illustrates boundary elements on cylindrical and cubical surfaces.

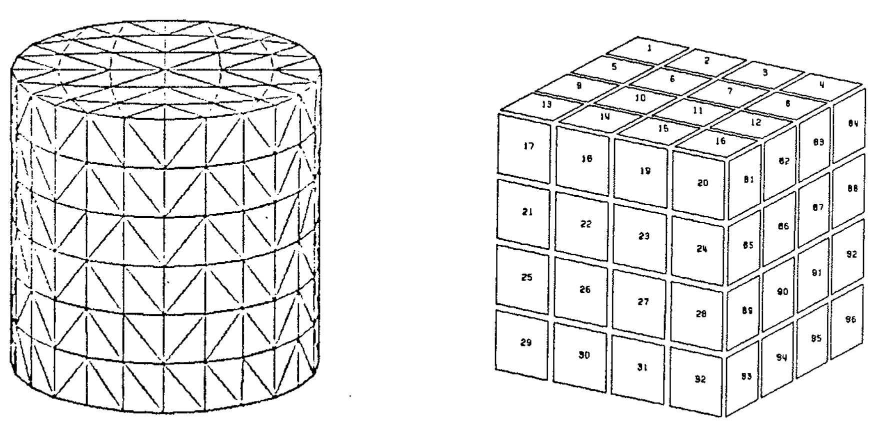

Figure 4.4: Boundary element models.

The unit sphere of the previous section is modelled with 32 cubic spline elements which are generated from second order continuous (case 1) and from positionally continuous (case 2) approximations. Figure 4.5 shows the cubic spline boundary element models for the above two cases and for a third case that will be considered in the following section.

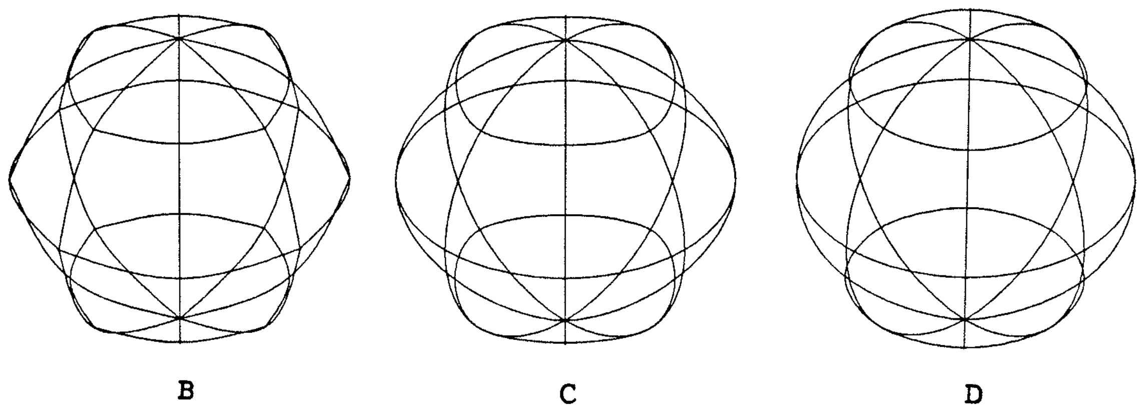

Figure 4.5: Cubic spline boundary element models of unit sphere.

The program has been used for element generation and data preparation in the boundary element method examples in this work as well as in [50].

4.2 BOUNDARY ELEMENT METHOD SOLUTIONS

In order to test the boundary element method a number of problems are considered. The first example aims at determining the performance of the numerical integration schemes. The second example illustrates the effect of geometrical modelling errors on the results. The third problem involves the computation of a field which is of nonlinear distribution. The last example is a multi-media problem.

A Mixed Boundary Value Problem

The problem is that of solving for the field in the interior of a cube with mixed boundary conditions on the surface. The particular choice of $\phi=1$ on the upper face, $\phi=0$ on the lower face and $\partial\phi/\partial n=0$ on the side faces yields a linear field distribution in the z-direction without a singularity in the interior. This example is a special one in that it illustrates one major advantage of the Green's theorem formulation over the simple layer formulation; that is since the exterior $\partial\phi/\partial n$ has singularities the simple layer formulation which solves for the interior and exterior fields simultaneously, has to model the charges with proper singular behaviour or, at least, with higher degree polynomials and with more elements; while no such complications exist for the Green's theorem formulation because it solves for the interior field only and $\partial\phi/\partial n$ has no singularities for the interior problem. The geometry, as shown in Figure 4.6, is modelled using 6 bi-cubic spline elements of Type III with 8 vertices. Note that the elements of Type II would model the same geometry with 32 vertices. It may be worth noting the relation between the global expansion functions w_i and the local shape functions W_i. Since there are 8 vertices, the number of global expansion functions is 8 but the number of global shape functions is 72 for there are 6 elements each with 12 local vertices.

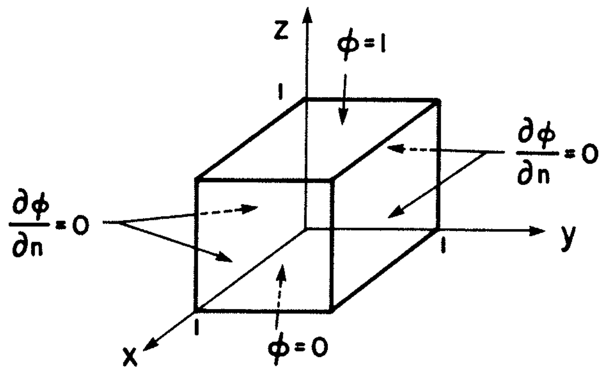

Figure 4.6: Geometry and boundary conditions for the mixed problem.

For the solution of the problem, the vertices where boundary conditions change, had to be doubled so as to let one vertex be associated with one condition only. This way the number of global expansion functions is increased to 16. In general, the number of global expansion functions can be increased up to the total number of global shape functions which is particularly useful when the field has discontinuities since this process relaxes the continuity condition on the unknowns without affecting the geometry definition. Therefore, in [38] if the nodes had been doubled so as to have one node be associated with one element only then exactly the same or better results would have been obtained with the linear elements as had been obtained with pulses. It may have been noticed that the concept exploits the independence of source representation from the geometry definition so as to provide for a subparametric modelling.

The results, given in Table 4.3, are obtained with 4-point quadrature and 6-point quadrature for the regular and the principal value integrations, respectively.

TABLE 4.3

Results for the mixed problem

potential	computed	exact
z=1.0	0.999881	1.000000
z=0.875	0.874909	0.875000
z=0.750	0.749938	0.750000
z=0.625	0.624967	0.625000
z=0.500	0.499995	0.500000
z=0.375	0.375024	0.375000
z=0.250	0.250053	0.250000
z=0.125	0.125081	0.125000
z=0.0	0.000111	0.000000
$\tilde{E}_{a,T}$	0.000119	----
$\tilde{E}_{a,1}$	0.000064	----
gradient		
z=1.0	0.999731	1.000000
z=0.0	-0.999664	-1.000000
$\tilde{E}_{a,T}$	0.000336	----
$\tilde{E}_{a,1}$	0.000302	----

Since the field variation is linear and there are no geometrical modelling errors, the results illustrate, in fact, merely the round-off errors and the accuracy of the numerical integrations. Further computations of the potential in the interior verified that the errors above are the largest to occur, as was expected due to the maximum principle, and that the numerical integrations have to be performed more accurately the closer to the boundary the point of potential computation.

Conducting Sphere in Free Space

In order to demonstrate the effect of geometrical modelling errors on the accuracy of the boundary element method solutions, the problem of calculating the field distribution due to a sphere in free space with $\phi = 1$ on the surface is considered. The analytical solutions are

$$\phi(r) = \frac{1}{r}$$
$$\frac{\partial\phi}{\partial n} = 1 \qquad (4.9)$$
$$\int_S \frac{\partial\phi}{\partial n}\, ds = 4\pi \ .$$

The unit sphere models of the previous section corresponding to case 1 with 8 elements and cases 2 and 1 with 32 elements are employed to obtain the results in columns A, B and C of Table 4.4, respectively. Inspection of the element corner nodes revealed that the center node in each subregion was off the spherical surface. Therefore, a fourth case (column D) is considered where a unit sphere is used, model D in Figure 4.5, which is modelled as in case C but with the center node of each subregion, one octant of the sphere, on the surface.

In all cases bi-cubic spline elements of Type III are used. The geometrical modelling errors, here, are slightly different than those given for the Coons patch approximation in the previous section since the bi-cubic spline elements are Coons patches themselves.

TABLE 4.4

Results for unit sphere in free space

ϕ at	A	B	C	D	exact
r= 2	.486169	.478177	.493983	.498977	.500000
r= 3	.323329	.318879	.328875	.332537	.333333
r= 4	.242335	.239164	.246519	.249376	.250000
r= 5	.193817	.191324	.197172	.199478	.200000
r= 6	.161492	.159415	.164297	.166216	.166667
r= 7	.138412	.136633	.140747	.142397	.142857
r= 8	.121104	.119530	.123118	.124565	.125000
r= 9	.107645	.106251	.109436	.110723	.111111
r=10	.096585	.095627	.098491	.099651	.100000
$\tilde{E}_{a,T}$	.013831	.021823	.006017	.001023	---
$\tilde{E}_{a,1}$	.006454	.009330	.002926	.000561	---
$\partial\phi/\partial n$ at (x,y,z)					
$(0,0,1)$	1.1238	1.2441	1.0695	1.0504	1.0000
$(\sqrt{\tfrac{1}{2}},0,\sqrt{\tfrac{1}{2}})$	1.0274	1.4017	1.2074	1.0776	1.0000
$(1,0,0)$	1.1485	1.2014	1.0282	1.0184	1.0000
$(\sqrt{\tfrac{1}{2}},\sqrt{\tfrac{1}{2}},0)$	1.0759	1.3512	1.0788	.99683	1.0000
$(\tfrac{1}{2},\tfrac{1}{2},\sqrt{\tfrac{1}{2}})$	.99102	1.1667	.94103	1.0657	1.0000
$E_{r,T}$	14.9%	40.2%	20.7%	9.17%	---
$E_{r,1}$	5.32%	10.5%	6.41%	2.92%	---
$\int_S \frac{\partial\phi}{\partial n}\,ds$	12.2184	12.0365	12.3556	12.5448	12.5664
$E_{r,T}$	2.77%	4.22%	1.68%	.172%	---

From the results above we deduce that since the geometrical model is inexact the normal derivative of the potential on the surface does not come out to be constant. Further, the inaccurate geometrical modelling in general and the derivative discontinuous approximation in particular degrades the results for $\partial\phi/\partial n$ more than those for ϕ.

One point worth noting is that in this example and possibly in many practical problems the unknown that is solved for is a constant which can be approximated with linear elements although the geometry involves curved surfaces which require higher order modelling. Thus a superparametric option is a practical facility to be included in the method. Ideally one would like to have options for various types of elements for geometry and sources with superparametric and subparametric representations.

Sphere in the Field of a Point Charge

In order to test the method in a problem in which the field variation is not linear the following example is considered. The problem, illustrated in Figure 4.7, is that of solving for the potential exterior to the unit sphere that is held at $\phi=1$ and is in the field of a point charge.

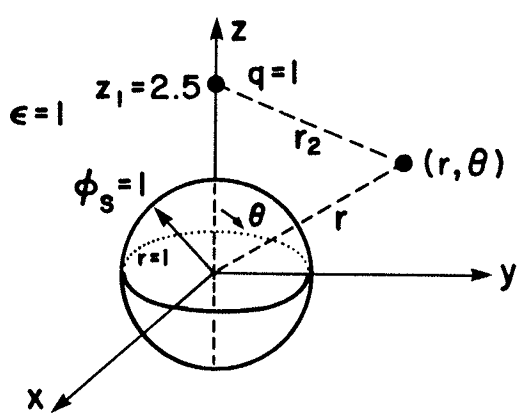

Figure 4.7: Unit sphere in the field of a point charge.

The analytical solutions from [19, p.202] are

$$\phi(r,\theta) = \frac{1}{4\pi\epsilon}\frac{q}{r_2} + \frac{r_1\phi_S}{r} - \frac{q}{4\pi\epsilon}\sum_{n=0}^{\infty}\frac{r_1^{2n+1}}{z_1^{n+1}}\frac{P_n(\cos\theta)}{r^{n+1}}$$

$$\left(\frac{\partial\phi}{\partial r}\right)_{r=r_1} = \frac{q}{4\pi\epsilon}\sum_{n=0}^{\infty}(2n+1)\frac{r_1^{n-1}}{z_1^{n+1}}P_n(\cos\theta) - \frac{\phi_S}{r_1} \tag{4.10}$$

$$\int_S \frac{\partial\phi}{\partial n}\,ds = \frac{-qr_1}{\epsilon z_1} + 4\pi\, r_1\, \phi_S \quad ,$$

where $P_n(\cos\theta)$ are the Legendre functions. The graphs of the numerical results and the analytical solutions are plotted in Figure 4.8.

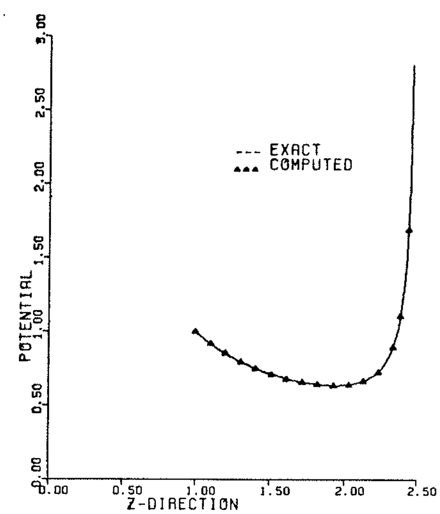

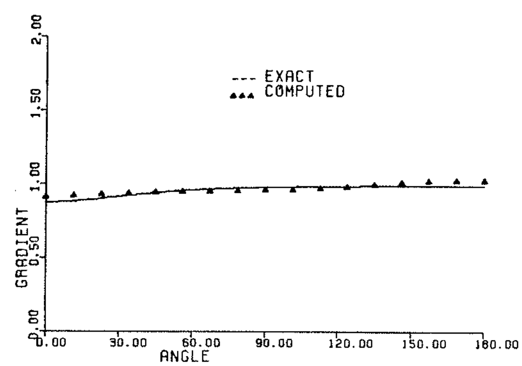

Figure 4.8: Graphs of results for the sphere and point charge.

Table 4.5 illustrates the exact and computed values at a number of points. The sphere model consists of 8 elements with 12 vertices adjusted so as to yield the least geometrical error positionally.

TABLE 4.5

Results for the sphere in the field of a point charge

potentials	computed	exact
z=1.24	.8333005	.8317143
z=1.49	.7204745	.7207277
z=1.74	.6546032	.6556654
z=1.99	.6371209	.6385273
z=2.24	.7336603	.7351963
z=2.49	8.342561	8.344123
$E_{a,T}$	.00409	---
$E_{a,1}$	.00136	---
$\partial\phi/\partial n$ on the sphere		
θ =0°	.91052	.87621
θ =45°	.94314	.94164
θ =90°	.95787	.97860
θ =135°	.99574	.98820
θ =180°	1.0247	.99025
$E_{a,T}$	.0374	---
$E_{a,1}$	.0206	---
$\int \frac{\partial\phi}{\partial n}\, ds$	12.1432	12.1664
$E_{r,T}$	.190%	---

A Multi-Media Problem

The method is also tested in a multi-region problem where the geometry and material properties are as illustrated in Figure 4.9. The inner sphere is held at ϕ =1. The analytical

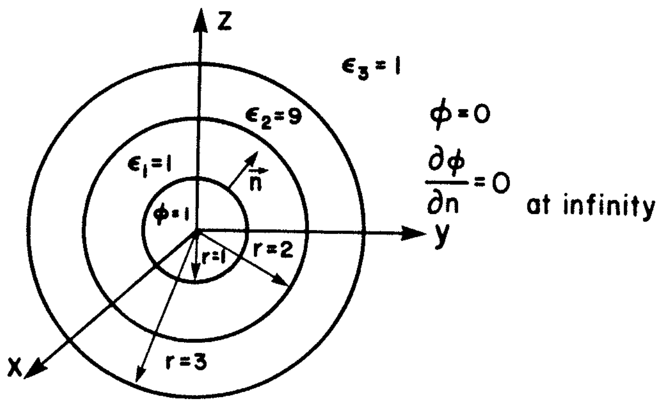

Figure 4.9: A multi-media problem.

solution for the potential is

$$\phi(r) = \begin{cases} \frac{1}{207}\left(\frac{243}{r} - 36\right) & 1 \le r \le 2 \\ \frac{1}{23}\left(\frac{3}{r} + 8\right) & 2 \le r \le 3 \\ \frac{1}{23}\left(\frac{27}{r}\right) & 3 \le r \end{cases} \tag{4.11}$$

The graph of (4.11) is plotted in Figure 4.10 where the numerical results are also indicated.

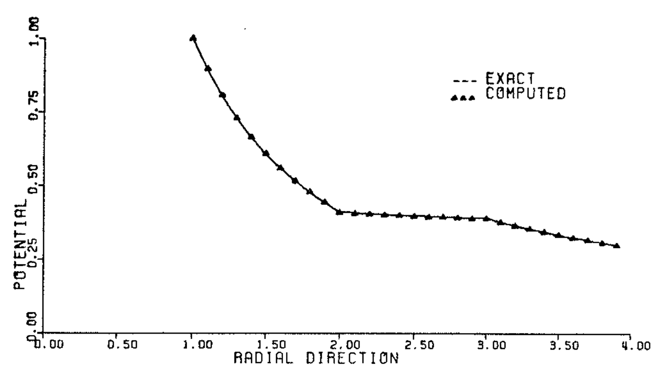

Figure 4.10: Graph of the potential for the multi-media problem.

The normal derivative of the potential and its integral on the spherical surfaces can be calculated exactly from

(4.11). Table 4.6 contains the results at a number of points with the associated errors in the radial direction along the x-axis.

TABLE 4.6

Results for the multi-media problem

potentials	computed	exact
r=1.2	.8072491	.8043479
r=1.5	.6098693	.6086957
r=1.8	.4793029	.4782609
r=2.0	.41097	.41304
r=2.3	.4027807	.4045368
r=2.7	.3943289	.3961352
r=3.0	.38876	.39130
r=3.3	.3550630	.3557312
r=3.8	.3080718	.3089245
$\tilde{E}_{a,T}$	.00399	---
$\tilde{E}_{a,1}$	.00150	---
$\partial\phi/\partial n$ on the spheres		
r=1.0	1.1995	1.1739
r=2.0−	−.28071	−.29348
r=2.0+	.031190	.032609
r=3.0−	−.014588	−.014493
r=3.0+	.13129	.13043
$E_{r,T}$	2.71%	---
$\int \frac{\partial\phi}{\partial n}\, ds_1$	14.756	14.752
$\int \frac{\partial\phi}{\partial n}\, ds_{2-}$	-14.748	-14.752
$\int \frac{\partial\phi}{\partial n}\, ds_{2+}$	1.6387	1.6391
$\int \frac{\partial\phi}{\partial n}\, ds_{3-}$	-1.6323	-1.6391
$\int \frac{\partial\phi}{\partial n}\, ds_{3+}$	14.691	14.752
$E_{r,T}$	0.413%	---

Chapter V

CONCLUSIONS

In this work, the mathematical theory, the numerical formulation and the application of a data preparation technique and of a boundary element method are shown. The data preparation method serves both the two-dimensional finite element and three-dimensional boundary element programs and provides at least first order continuous geometrical modelling by utilizing B-spline approximation and interpolation and the Coons patch methodology. The boundary element method caters to piecewise homogeneous Laplacian fields in three-dimensional space by employing the Green's theorem representation of the potential, the Galerkin scheme of solution for the unknowns and the bi-cubic spline elements which combination brings about an unique method. A number of variations of two-dimensional and three-dimensional spline elements are derived and tested, and numerical techniques have been adopted for the evaluation of principal value integrals and integrals with nearly singular integrands. Below are further conclusions and recommendations regarding both methods.

5.1 DATA PREPARATION

The data preparation method is based on a sub-regional mesh generation scheme which provides a number of advantages. The region can be divided into a number of subregions so as to comply with the differing material properties and boundary conditions. This enables grouping of elements with some common property into aggregates for convenient reference. A distinct need for subregional mesh generation becomes apparent in the case of three-dimensional boundary element generation on free-form surfaces. That is, wherever the surface needs to be modelled more accurately more subregions can be taken there so as to supply more information. The algorithm is fast, requires minimal effort from the user and very little array storage, and provides precise modelling of problem geometry, good correlation between input and output as well as well-conditioned elements and reduced data preparation time. The method handles complex surfaces, eliminates human error, is applicable to a broad range of problems and provides for second order continuous modelling of subregions and at least first order continuous modelling of the whole surface. Completely second order continuous modelling can be achieved by an algorithm that works on subcurves rather than on subregions. However, the efficiency of the Coons patch form is questionable for it yields vanishing cross-derivatives at corners. It is possible to replace the Coons patch technique with bi-variate B-spline basis functions obtainable through tensor product of uni-variate B-spline basis [16]. The user-friendliness of the method can be improved upon by introducing a command language and graphical input through tablet.

The method of mesh generation is readily applicable to geometric design of free-form surfaces and their display on the screen. When generalized to higher dimensions, the method may be used to approximate m-dimensional manifolds in (m+1)-dimensional spaces. For example, conductivity or temperature distributions as functions of two coordinates and also equi-function surfaces in three-dimensional space may be modelled. As well, tri-variate, i.e. volumetric, finite elements may be generated.

5.2 FIELD SOLUTION

The conlusions regarding the boundary element method can be grouped into three sections: the expansion functions, the Green's theorem formulation and the Galerkin solution. In this work the geometry and the unknowns are modelled with bi-cubic spline elements which provide smooth modelling, high order approximation and vertex sharing. However, it has been found that the employment of spline elements decreased the practicality of the method as follows. The controlling vertices of the spline element do not necessarily lie on the boundary. Therefore, it is difficult to estimate the effect of changing the location of a controlling vertex on the geometry. While, since the defining points for a Lagrangian or Serendipity element are always on the surface, relocating a point introduces an easily identifiable modification to the model. The shape functions of the bi-cubic spline element are located with respect to each other not in the most desirable form. The isoparametric usage of cubic-spline element for all types of problems and desired accuracies is not justified in some applications while the Lagrangian or Serendipity elements offer a choice between shorter run time, with crude results sometimes, and longer execution time with accurate results, usually. Vertex sharing among spline elements did not prove to be an advantage in the problems with mixed boundary condition or media for in these cases vertices shared by elements with different boundary conditions or around dissimilar media must be decoupled. Further, in practical applications the surfaces are too involved to be modelled by a few spline elements. It is rather desirable to employ low order elements but many of them. High order modelling is costly because it requires a high order quadrature scheme and also contains too many unknowns per element. Another argument against using few high order elements is that when the point of potential computation is close to the boundary the integrations become more difficult to handle. The spline elements are that subset of Lagrangian elements which provide second order continuity. Hence if the data preparation method is used then all cubic elements generated will provide second order continuous representation wherever the geometry is modelled as such.

As regards the Green's theorem formulation the advantages and disadvantages of the method in comparison with the simple layer formulation can be stated as follows. First it should be noted that a two step procedure is followed in both formulations, i.e. from given boundary conditions some unknowns on the boundary are solved for and then the potential is calculated at points in the region. The simple layer formulation requires lower order continuity of the unknowns than the Green's theorem formulation. On the other hand, the simple layer formulation has to model the charges with the proper singular behaviour whenever either the interior or the exterior problem has singularities while the Green's theorem formulation does not model the normal derivative of the potential singularly if the field in the region of interest does not have singularities. Also the determination of the singularity in the normal derivative of the potential is easier than the determination of the charge singularity. Two coefficient matrices that are block-sparse and are independent of given boundary conditions are generated in the Green's theorem formulation while one dense coefficient matrix and a boundary condition dependent right-hand side is generated in the simple layer formulation. The generation of these coefficient matrices is the most time-consuming part in a boundary element program.

Further, in the Dirichlet problem with homogeneous medium, simple layer formulation does not involve an integration of a term with $\partial/\partial n(1/R)$ while the Green's theorem formulation includes such an integration regardless of the type of the problem.

At the second step potential or its derivatives are calculated. The Greens' theorem formulation involves two integrals around the region in which the potential is computed while simple layer formulation uses one integral and integrates over all elements in the problem. Though the Green's theorem formulation seems to be advantageous in this respect in practice the determination of the region the point of potential computation is in requires a point-region search which is an unnecessary algorithmic burden. The computation of potentials is easier in the simple layer formulation since there is no $\partial/\partial n(1/R)$ integration involved and the potential is continuous at the boundary while the potential jumps by $\phi/2$ in the Green's theorem formulation. In general the computation of the derivatives of the potential is easier with the simple layer formulation except for the normal derivative of the potential on the boundary which is obtained in the Green's theorem formulation in the first step.

The Galerkin method has been found to be more stable than point matching but computationally more costly because of the additional outer integral.

Appendix A

AIR BUBBLE IN DIELECTRIC SLAB

Air bubbles in an insulating material are known to reduce its quality. In order to determine the field distribution inside and around an insulator that contains an air bubble the following problem is modelled and solved.

The geometry of the problem with the boundary elements is shown in Figure 5.1. The porcelain insulator block (ϵ_r=6) is 6 by 5 by 4 units and it is contained in the region defined by $-4 < z < 2$, $-3 < y < 2$ and $-2 < x < 2$. The spherical air

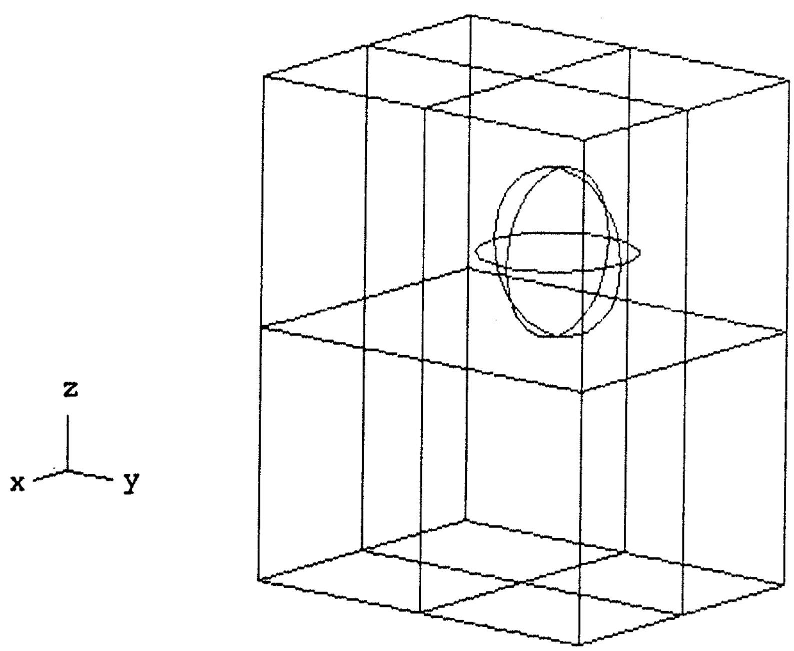

Figure 5.1: The boundary element model.

bubble (ϵ_r=1.0006) of unit radius is centered at x=y=z=0.

The upper surface of the insulator is held at 1 volt while the lower surface is at 0 volts. Figure 5.2 shows the equipotential lines in increments of 1/13 volt, in a cros-sectional frame, at x=0, which extends from y=-5 to y=5 hor-

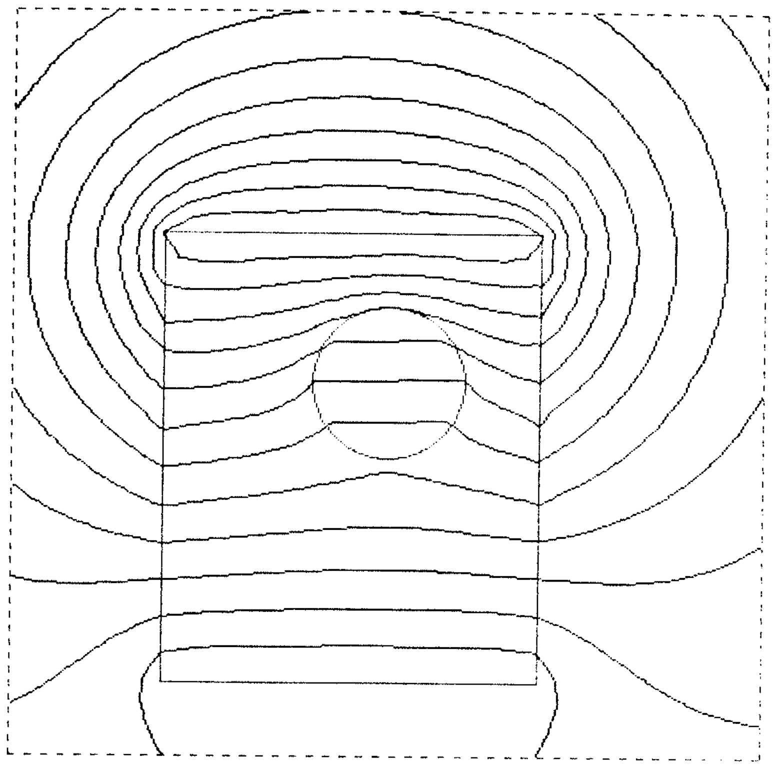

Figure 5.2: Equipotential lines.

izontally and from z=-5 to z=5 vertically. Small inaccuracies in equipotential lines are partly due to the interpolations in the contour plotting program.

Figure 5.3 shows the graph of the potential along the z-axis from z=-5 to z=5.

The problem has been modelled with 32 elements and 146 vertices. The solution is obtained in 108 minutes on an IBM

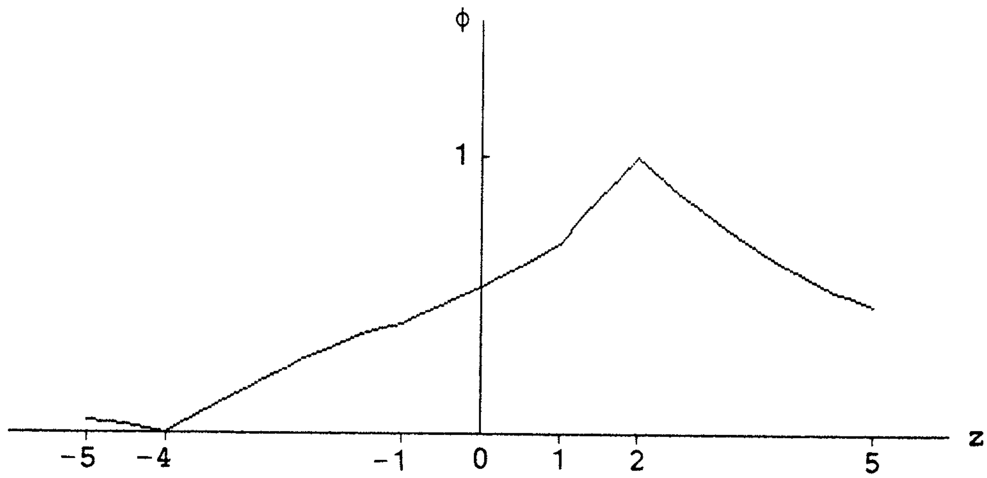

Figure 5.3: Graph of voltage along the z-axis

PC/XT computer, runnig MS-FORTRAN Version 3.2 under MS-DOS Version 2.10. The figures are drawn in 640 by 400 screen resolution and hardcopies are produced with an EPSON FX-80 dot matrix printer.

REFERENCES

1. Forsythe, G.E. and Wasow, W.R. Finite-Difference Methods for Partial Differential Equations. New York: John Wiley & Sons, 1960.

2. Fox, L. Numerical Solution of Ordinary and Partial Differential Equations. Reading, Massachusetts: Pergamon Press, 1962.

3. Zienkiewicz, O. C. The Finite Element Method in Engineering Science. New York: McGraw-Hill, 1971.

4. Pinder, G.F. and Gray, W.G. Finite Element Simulation in Surface and Subsurface Hydrology. New York: Academic Press, 1977.

5. Wexler, A. Finite Elements For Technologists. Tech. Rept. TR80-4, Dept. of Elec. Eng., University of Manitoba, Canada, 1973.

6. Decreton, M.C. Treatment of Singularities In the Finite Element Method. M.Sc. Thesis, Dept. of Elec. Eng., University of Manitoba, Canada, October 1972.

7. Wexler, A. Perspectives on the Solution of Simultaneous Equations. Tech. Rept. TR79-2, Dept. of Elec. Eng., University of Manitoba, Canada, 1979.

8. Prenter, P.M. Splines and Variational Methods. New York: John Wiley & Sons, 1975.

9. Schultz, M.H. Spline Analysis. Englewood Cliffs, N.J.: Prentice-Hall, 1973.

10. Dahlquist, G. and Bjork, A. Numerical Methods. Englewood Cliffs, N.J.: Prentice-Hall, 1974.

11. Coons, S.A. "Surface Patches and B-Spline Curves", Computer Aided Geometric Design. R.E. Barnhill and R.F. Riesenfeld (eds), New York: Academic Press, 1974.

12. Gordon, W.J. and Riesenfeld, R.F. "B-spline Curves and Surfaces", Computer Aided Geometric Design. R.E. Barnhill and R.F. Riesenfeld (eds), New York: Academic Press, 1974.

13. Haber, R. et al. "A General Two-Dimensional, Graphical Finite Element Preprocessor Utilizing Discrete Transfinite Mappings', International J. for Num. Methods in Eng., Vol. 17, 1981.

14. Zienkiewicz, O.C. and Phillips, D.V. "An Automatic Mesh Generation Scheme for Plane and Curved Surfaces by 'Isoparametric' Co-ordinates", International J. for Num. Methods in Eng., Vol. 3, 1971.

15. Gordon, W.J. and Hall, C.A. "Construction of Curvilinear Co-ordinate Systems and Applications to Mesh Generation", International J. for Num. Methods in Eng., Vol. 7, 1973.

16. Barsky, B.A. and Greenberg, D.P. "Determining a Set of B-spline Control Vertices to Generate an Interpolating Surface", Computer Graphics and Image Processing. Vol. 14, pp. 203-226, 1980.

17. Barnhill, R.E. "Coon's Patches" Computers in Industry. Vol. 3, pp. 37-43, 1982.

18. Rogers, D.F. and Adams, J.A. Mathematical Elements for Computer Graphics. New York: McGraw-Hill, 1976.

19. Stratton, J.A. Electromagnetic Theory. New York: McGraw-Hill Book Co., 1941.

20. Kellog, O.D. Foundations of Potential Theory. Berlin: Verlag von Julius Springer, 1929.

21. Sternberg, W.J. and Smith, T.L. The Theory of Potential and Spherical Harmonics. Toronto, Canada: The University of Toronto Press, 1944.

22. Courant, R. and Hilbert, D. Methods of Mathematical Physics. Vol. 1, New York: Interscience Publishers, 1966.

23. Courant, R. and Hilbert, D. Methods of Mathematical Physics. Vol. 2, New York: Interscience Publishers, 1966.

24. Jaswon, M.A. and Symm, G.T. Integral Equation Methods In Potential Theory and Elastostatics. New York: Academic Press, 1977.

25. Knops,R.J. and Payne, L.E. Uniqueness Theorems in Linear Elasticity. Berlin: Springer-Verlag, 1971.

26. Tsuji, M. Potential Theory in Modern Function Theory. Tokyo: Maruzen, 1959.

27. Stakgold, I. Boundary Value Problems of Mathematical Physics. Volume 1, New York: Macmillan Co., 1967.

28. Stakgold, I. Green's Functions and Boundary Value Problems. New York: John Wiley & Sons, 1979.

29. Kreyszig, E. Introductory Functional Analysis with Applications. New York: John Wiley & Sons, 1978.

30. Zabreyko, P.P. et al. Integral Equations. Leyden, Netherlands: Noordhoff International Publishing, 1975.

31. Finlayson, B.A. The Method of Weighted Residuals and Variational Principles. New York: Academic Press, 1972.

32. Mikhlin, S. G. Variational Methods In Mathematical Physics. New York: Pergamon Press, 1964.

33. Mikhlin, S.G. Integral Equations. New York: Pergamon Press, 1964.

34. Mikhlin, S.G. and Smolitskiy, K.L. Approximate Methods for Solution of Differential and Integral Equations. New York: Elsevier, 1967.

35. Mikhlin, S.G. The Numerical Performance of Variational Methods. Groningen, The Netherlands: Wolters-Noordhoff, 1971.

36. Krasnosel'skii, M.A. et al. Approximate Solution of Operator Equations. Groningen, The Netherlands: Wolters-Noordhoff, 1972.

37. Harrington, R.F. Field Computation by Moment Methods. Reprinted by R.F. Harrington, R.D.2, West Lake Road, Cazenovia, N.Y., 1968.

38. Harrington, R.F. et al. "Computation of Laplacian Potentials by an Equivalent Source Method", Proceedings IEE, Vol. 116, No. 10, 1715-1720, October 1969.

39. Ivanov, V.V. The Theory of Approximate Methods and Their Application to the Numerical Solution of Singular Integral Equations. Leyden: Noordhoff, 1976.

40. Morse, P.M. and Feshbach, H. Methods of Theoretical Physics. Volumes 1,2. New York: McGraw-Hill, 1953.

41. Jeng, G. and Wexler, A. "Self-Adjoint Formulation of Problems Having Non-Self-Adjoint Operators", IEEE Trans. On Microwave Theory and Techniques, Vol. MTT-26, No.2, February 1978.

42. Tricomi, F.G. Integral Equations. New York: Interscience Publishers, Inc, 1957.

43. Vulikh, B.Z. Introduction to Functional Analysis. New York: Pergamon Press, 1963.

44. Wendland, W.L. "On Galerkin Collocation Methods for Integral Equations of Elliptic Boundary Value Problems", Numerical Treatment of Integral Equations. ISNM 53, J. Albrecht and L. Collatz (eds.), Stuttgart: Birkhauser Verlag, 1980.

45. Stroud, A.H. and Secrest, D. Gaussian Quadrature Formulas. Englewood Cliffs, N. J.: Prentice-Hall, 1966.

46. Lachat, J.C. and Watson, J.O. "Effective Numerical Treatment of Boundary Integral Equations: a Formulation for Three-Dimensional Elastostatics", International J. for Num. Methods in Eng. Vol. 10, pp.991-1005, 1976.

47. McDonald, B.H., Friedman, M. and Wexler, A. "Variational Solution of Integral Equations", in IEEE Trans. On Microwave Theory and Techniques, Vol. MTT-22, No. 3, March 1974.

48. McDonald, B.H. Constrained Variational Solution of Field Problems. Ph.D. Thesis, University of Manitoba, Canada, 1975.

49. Lean, M.H. Electromagnetic Field Solution with the Boundary Element Method. Ph.D. Thesis, Tech. Rept. TR81-5, Dept. of Elec. Eng., University of Manitoba, Canada, 1981.

50. Bilgen, S. Cubic Spline Elements for Boundary Integral Equations. Ph.D. Thesis, Tech. Rept. TR82-5, Dept. of Elec. Eng., University of Manitoba, Canada, 1982.

51. Klimpke, B.W. A Two-Dimensional Multi-Media Boundary Element Method. M.Sc. Thesis, Tech. Rept. TR83-2, Dept. of Elec. Eng., University of Manitoba, Canada, 1983.

52. Anderssen, R.S. et al. The Application and Numerical Solution of Integral Equations. The Netherlands: Sijthoff and Noordhoff, 1980.

53. Crouch, S.L. and Starfield, A.M. Boundary Element Methods in Solid Mechanics. London: George Allen & Unwin, 1983.

54. Ligget, A.L. and Liu, P.L-F. The Boundary Integral Equation Method For Porous Media Flow. Boston: George Allen & Unwin, 1983.

55. Yildir, Y.B. and Wexler,A. MANDAP, a FEM/BEM Data Preparation Package - User's Manual. Tech. Rept. TR82-4, Dept. of Elect. Eng., University of Manitoba, 1982.

56. Wexler, A. et al. MANFEP User's Manual. Tech. Rept. TR79-1, Dept. of Elect. Eng., University of Manitoba, 1979.

57. Yildir, Y.B. et al. Ontario Hydro-GPU HVDC Interconnection Ground Electrode Study. Tech. Rept. TR82-1, Dept. of Elec. Eng., University of Manitoba, 1982.

58. Yildir, Y.B. et al. Techniques for Improving Computational Efficiency of the Numerical Electromagnetic Code (NEC) - Part II. Tech. Rept. TR82-2, Dept. of Elect. Eng., University of Manitoba, 1982.

59. Yildir, Y.B. and Wexler, A. MANBEP4 - A Boundary Element Method Program for the Solution of Laplace's Equation in Three-Dimensional Space. Tech. Rept., Dept. of Elect. Eng., University of Manitoba, 1983.

60. Wexler, A. et al. Field Distribution from a Thin Film Head Using the Finite Element Method. Research Project Report to XEROX, TASC Ltd., Winnipeg, 1981.

61. Yildir, Y.B. and Wexler,A. "MANDAP - A FEM/BEM Data Preparation Package", IEEE Trans. on Magnetics. November, 1983.

62. Berezin, I.S. and Zhidkov, N.P. Computing Methods Vol. 1, London: Pergamon Press, 1965.

63. Shaw, J.G. Numerical Analysis of Semiconductor Devices. Ph.D. Thesis, Tech. Rept. TR83-6, Dept. of Elec. Eng., University of Manitoba, Canada, 1983.